Archive of Applied Mechanics (2021) 91:883–917
https://doi.org/10.1007/s00419-020-01794-0

ORIGINAL

S. W. Yang · Y. X. Hao · L. Yang · L. T. Liu

Nonlinear vibrations and chaotic phenomena of functionally graded material truncated conical shell subject to aerodynamic and in-plane loads under 1:2 internal resonance relation

Received: 16 April 2020 / Accepted: 17 September 2020 / Published online: 9 October 2020

Abstract This paper focuses on the nonlinear dynamic responses of a functionally graded material (FGM) truncated conical shell under 1:2 internal resonance relation. The FGM truncated conical shell is subjected to the in-plane load and the aerodynamic load along the meridian direction. According to a power-law distribution, the material properties are assumed to be modified along the thickness direction smoothly and continuously and the material properties are temperature dependent. The aerodynamic load is obtained by the first-order piston theory with the curvature correction term. According to von Karman type nonlinear geometric relations, first-order shear deformation shell theory, Hamilton principle, the nonlinear equations of motion for the FGM truncated conical shell are established. Furthermore, the nonlinear equations of motion are reduced into a system of the ordinary differential equations by utilizing Galerkin procedure. The multiple scales method is used to obtain the averaged equations for the FGM truncated conical shell under the relations of 1:2 internal resonance and 1/2 subharmonic resonance. The frequency–response curves, time history diagrams, phase portraits, Poincare maps and bifurcation diagrams with different parameters are yielded by employing numerical calculations. The influences of exponent of volume fraction, Mach number, damping coefficient and in-plane load on the nonlinear resonance behaviors of the FGM truncated conical shell are investigated. The chaotic and periodic motions of the FGM truncated conical shell have been discussed in detail.

Keywords Nonlinear vibrations · Chaos · Functionally graded materials · 1:2 Internal resonance · Conical shell

1 Introduction

Functionally graded materials (FGMs) are famous for their excellence thermomechanical performances, and the FGM structures inspired researchers to explore the dynamics which are often used in the high strength or high temperature environments [1,2]. Because of the continuous and smooth varies of the volume fractions of the constituent materials for the functionally graded materials, the material properties, for example the

S. W. Yang · Y. X. Hao (✉) · L. Yang · L. T. Liu
College of Mechanical Engineering and Beijing Key Laboratory of Electromechanical System Measurement and Control, Beijing Information Science and Technology University, Beijing 100192, People's Republic of China
E-mail: bimhao@163.com

S. W. Yang
E-mail: shaowu_yang@163.com

L. Yang
E-mail: yangli9087@126.com

L. T. Liu
E-mail: ltliu0@163.com

Young's modulus, the thermal expansion coefficient and the density, all change continuously. Therefore, the FGM structures can relieve the problems of the interfacial debonding and the stress concentration. It is well known that the conical shell structure is one of the primary structures in many engineering community, for example, aircraft and rocket propulsion system, ship structures, pressure and piping vessels [3,4]. The FGM conical shells are often subjected to the complex loads, for example aerodynamic load, in-plane load, transverse load and thermal stress, which will result in the complex nonlinear dynamics. Particularly, the occurrence of the nonlinear internal resonance phenomenon can cause the large amplitude vibration, noises, irrecoverable deformations and cracks in practical engineering applications, even the failure of the structures. In the early days, the resonances leaded to the collapse of the 860 m Taksim bridge in the USA. Therefore, it is significant to predict and understand the nonlinear dynamic characteristics of FGM conical shell with internal resonance under complex loads.

Now, much researches have been carried out for the vibration characteristics of FGM conical shells. Javani et al. [5] performed a thermally induced vibration analysis for a functionally graded material conical shell which is considered the uncoupled thermoelasticity assumptions. The effects of the thickness upon the deflections, the semi vertex angle, geometrical nonlinearity, the length and the temperature dependency of the conical shells are investigated. Based on the higher-order shear deformation theory, Ansari et al. [6] investigated the large-amplitude free and forced vibrations of functionally graded carbon nanotube reinforced composite conical shells. Chan et al. [7,8] investigated the nonlinear dynamic responses and vibrations of truncated eccentrically stiffened functionally graded conical shells and truncated functionally graded conical panels surrounded by the elastic medium in the thermal environment. The influences of elastic foundations, dimensional parameters, inhomogeneous, temperatures and outside stiffeners on the nonlinear vibration and dynamic response of the truncated conical shells are investigated. Dai et al. [9] studied the frequency characteristics of the rotating truncated conical shells by using the Haar wavelet method. The vibration behaviors of a truncated conical sandwich shell that include temperature-dependent homogeneous core and porous behavior in the various thermal conditions are investigated by Rahmani et al. [10].

Song et al. [11] investigated the free vibrations of a truncated conical shell under the inertia force and elastic constraints with the arbitrary boundary conditions. Hao et al. [12,13] investigated the nonlinear vibration and supersonic flutter of a FGM circular conical panel by using the first order shear deformation theory. Sofiyev [14] provided the review on the buckling and vibration of functionally graded materials, functionally graded sandwich-conical shell, functionally graded layered conical shell and functionally graded conical shell. Jooybar et al. [15] investigated the effects of the geometrical parameters, the thermo environment, and graded index of the materials on free vibration of FGM conical panel by using differential quadrature method. Hao et al. [16] researched on the truncated metal-ceramic graded conical shell on aero-thermo-elastic flutter characteristics subjected to aerodynamic pressure and aerodynamic heating. Using Hamilton's principle and first-order shear deformation theorem, the equilibrium equations of two joined laminated conical shells were derived by Izadi et al. [17], and the free vibration analyses of the shells were investigated. Zhao et al. [18] presented a spectro-geometric-Ritz solution for the free vibration analyses of conical-cylindrical-spherical shell combinations with the arbitrary boundary conditions.

In the past few years, much researchers have interested in buckling characteristics of the conical shells. Sofiyev et al. [19,20] studied the dynamic stability of the functionally graded truncated conical shells and the FG orthotropic conical shells by using FSDT. Hoa et al. [21] investigated the nonlinear thermomechanical buckling and postbuckling of the ES-FGM truncated conical shells. The influences of the temperature, the stiffeners, the foundations, the material properties, the geometric dimensions on the stability of shells are given. Based on the classical shell theory, Chan et al. [22] provided a nonlinear static analysis for a truncated functionally graded carbon nanotubes-reinforced composite conical shells subjected to the axial load. Then, Chan et al. [23] studied the nonlinear buckling characteristics of truncated stiffened FGM conical shells subjected to a uniform axial compressive load and resting on the elastic foundation by using first-order shear deformation theory. The buckling analyses of the composite laminated conical shells reinforced with graphene sheets are investigated by Kiani [24]. Jiao et al. [25] proposed a semi-analytical approach to investigate dynamic buckling characteristics of the composite cylindrical shell reinforced by functionally graded carbon nanotubes under the dynamic displacement loads. Talebitooti [26] investigated the buckling of the composite sandwich conical shells subjected to a uniform external lateral pressure based on the first-order shear deformation shell theory.

Dung et al. [27] studied the buckling behaviors of a FGM truncated conical shell, the influences of stiffeners, dimensional parameters and material properties and discussed in detail. Zhao et al. [28] investigated the thermal-mechanical buckling characteristics of a FGM conical panel by using the element-free KP-Ritz method. Pasqua et al. [29] studied the buckling characteristics of the composite conical shell subject to different disturbed loads.

According to FSDT, the buckling behaviors of a composite sandwich conical shell subject to uniform external lateral load was given by Talebitooti [30]. Maali et al. [31] studied the buckling behaviors of a thin imperfection conical panel under the simply supported condition. According to the modified Donnell shell theory, Sofiyev et al. [32] investigated the thermo-elastic buckling of a FGM conical shell. The nonlinear temperature increase along the thickness direction was considered by them. Bich et al. [33] studied the linear buckling of the FGM conical panels subject to the external and axial pressures.

The improved double Fourier series has been widely used in vibration analysis of the beam, plate and shell structures under elastic boundary conditions or arbitrary boundary conditions with elastic supported. For example, Shi and Wang et al. [34–38] carried out a lot of researches on the vibration analyses of beam, plate and shell structures under the arbitrary boundary conditions by using the improved double Fourier series. According to an accurate modified Fourier series solution, the free vibration analyses of the truncated conical shells with general elastic boundary conditions were presented by Jin et al. [39]. Dai et al. [40] investigated dynamic behavior of cylindrical shell structures with general boundary condition based on the modified Fourier series method.

Zhang et al. [41–44] carried out a lot of studies on internal resonance behaviors of composite plate and shell structures, and their research results show that internal resonance has a great influence on the nonlinear vibration of plate and shell structures. Our group has done a lot of research on the shell and plate structures by using the techniques in this paper. For example, we have investigated the nonlinear vibration [3,4] and nonlinear flutter [12,16] of the FGM truncated conical shell and the nonlinear internal resonance behaviors of the FGM cylindrical shell [44]. Therefore, the method used in this paper is effective for dealing with the nonlinear dynamics problem of the FGM truncated conical shell.

Up to now, few researches have been carried out the nonlinear resonance behaviors of the FGM truncated conical shell with 1:2 internal resonance. In this paper, the nonlinear dynamics of a FGM truncated conical shell which is subjected to in-plane load and aerodynamic load under 1:2 internal resonance condition are investigated. Based on Hamilton principle, von Karman type nonlinear relations and FSDT, the nonlinear governing equations of motion for the FGM truncated conical shell are established. By using the Galerkin method, the ordinary differential equations of motion along the radial displacement are obtain. The qualification which the 1:2 internal resonance occurs of the FGM truncated conical shell is found. The multiple scales method is used to obtain the averaged equations for the FGM truncated conical shell under the relations of 1:2 internal resonance and 1/2 subharmonic resonance. The frequency-response curves, time history diagrams, phase portraits, Poincare maps and bifurcation diagrams with different parameters are yielded by employing numerical calculations to show the complex nonlinear dynamics and chaotic phenomena of the FGM truncated conical shell. The influences of exponent of volume fraction, Mach number, damping coefficient and in-plane load on the nonlinear resonance behaviors on the nonlinear vibrations of the FGM truncated conical shell are studied. The chaotic and periodic motions of the FGM truncated conical shell have been discussed in detail.

2 Equations of motion

Figure 1 shows the model of a FGM truncated conical shell. The geometric parameters of the FGM truncated conical shell are as follows: semi-vertex angle β, thickness h, length L and minor inner radius r_1. The radius of any point along the meridional are computed by $R = r_1 + x \sin\beta$. The curvilinear coordinate system $(x,\ \theta,\ z)$ is along the meridional, circumferential and radial directions, respectively, which is located on the mid-surface of the FGM truncated conical shell. It is considered that the FGM truncated conical shell is subjected to the in-plane load and aerodynamic load. The uniformly distributed in-plane load which at the two ends $x = 0$ and $x = L$ of the FGM truncated conical shell is represented as $p_1 \cos(\Omega t)$.

Considering the supersonic flow is parallel to the outside of the FGM truncated conical shell. Based on the first-order piston theory with the curvature correction term, the aerodynamic load P_a are approximated as [45,48].

$$P_a = -\frac{\gamma_a p_\infty M_a^2}{\sqrt{M_a^2 - 1}}\left[\frac{\partial w}{\partial x} + \left(1 - \frac{1}{M_a^2 - 1}\right)\frac{1}{M_a a_\infty}\frac{\partial w}{\partial t} - \frac{w}{2R\sqrt{M_a^2 - 1}}\right], \tag{1}$$

where last term is the curvature correction term, M_a, a_∞, p_∞, γ_a and t are Mach number, free stream velocity of sound, free stream static pressure, adiabatic exponent and time, respectively.

The material properties are regarded as varying continuously and smoothly along the thickness direction z according to a power law distribution. Thus, the outside surface of the FGM truncated conical shell is ceramic

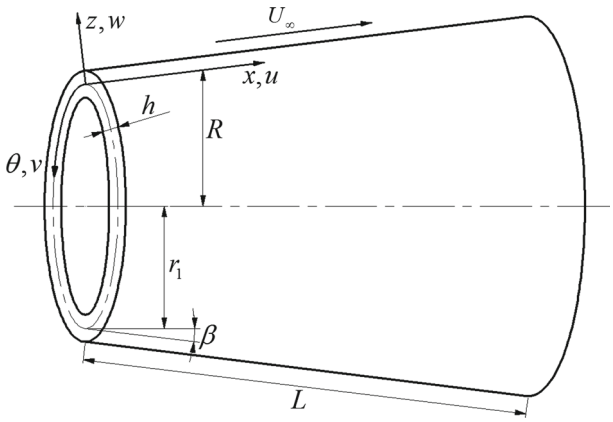

Fig. 1 The model of a FGM truncated conical shell is given

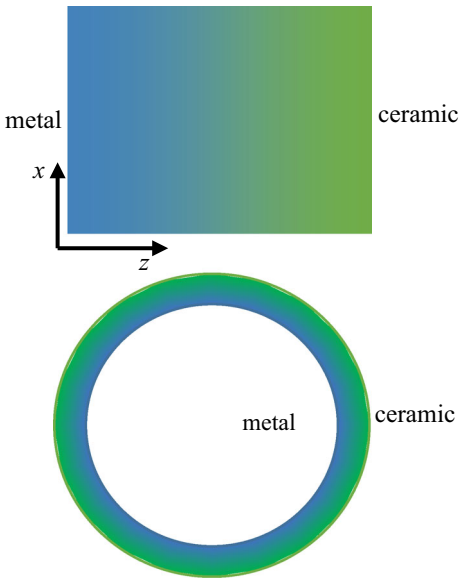

Fig. 2 The schematic diagram of the volume fractions of the ceramic and the metal for the FGM truncated conical shell through the thickness direction is obtained

rich. At the same time, the internal surface is metal rich. The schematic diagram of the volume fractions of the ceramic and the metal for the FGM truncated conical shell through the thickness direction is given in Fig. 2. The volume fractions of the ceramic and the metal for the truncated FGM conical shell is shown in Fig. 3, and they are written as follows

$$V_c(z) = \left(\frac{2z+h}{2h}\right)^{\eta}, V_m(z) = \left(\frac{h-2z}{2h}\right)^{\eta}, \tag{2}$$

where V is the volume fraction, the subscripts c and m represent ceramic and metal, respectively, and the superscript η is the volume fraction index of the ceramic.

The value of the Poisson's ratio ν of the FGM truncated conical shell is regarded as a constant. The other material properties of the FGM truncated conical shell, such as mass density ρ, Young's modulus E and coefficient of the thermal expansion α, are determined according to a linear rule of mixture as [49]

$$P = P_c V_c + P_m V_m, \tag{3}$$

The typical temperature-dependent material properties can be expressed as [50]

$$P_i = P_0\left(P_{-1}T^{-1} + 1 + P_1 T + P_2 T^2 + P_3 T^3\right), i = c,\ m, \tag{4}$$

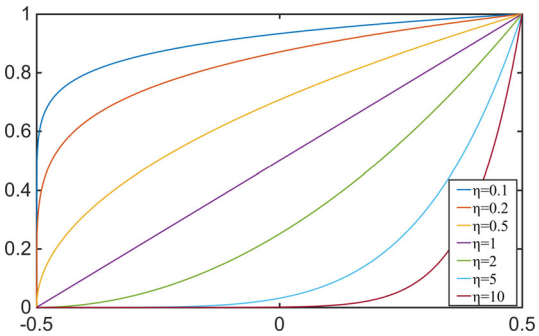

Fig. 3 The volume fractions of the ceramic through the thickness direction are obtained

where the temperature coefficients P_0, P_{-1}, P_1, P_2 and P_3 are the coefficients of the temperature T expressed in Kelvin. These coefficients are different for different constituent materials.

According to the first-order shear shell deformation theory [51], the displacement fields of the FGM truncated conical shell are assumed as

$$u(x,\theta,z,t) = u_0(x,\theta,t) + z\varphi_x(x,\theta,t), \tag{5a}$$

$$v(x,\theta,z,t) = v_0(x,\theta,t) + z\varphi_\theta(x,\theta,t), \tag{5b}$$

$$w(x,\theta,z,t) = w_0(x,\theta,t), \tag{5c}$$

where u, v and w stand for the displacements of any point in the x, θ and z directions, respectively, which are the functions of the middle in-plane displacements u_0, v_0 and w_0 of the FGM conical shell and the mid-surface rotations φ_x and φ_θ of the θ axis and the x axis, respectively.

Using the von Karman geometric nonlinear strain–displacement relationships, the nonlinear strains can be obtained as [52,53]

$$\varepsilon_x = \frac{\partial u_0}{\partial x} + z\frac{\partial \varphi_x}{\partial x} + \frac{1}{2}\left(\frac{\partial w_0}{\partial x}\right)^2, \tag{6a}$$

$$\varepsilon_\theta = \Re\frac{\partial v_0}{\partial \theta} + z\Re\frac{\partial \varphi_\theta}{\partial \theta} + \Re w_0\cos\beta + \Re\left(u_0 + z\varphi_x\right)\sin\beta + \frac{1}{2}\Re^2\left(\frac{\partial w_0}{\partial \theta}\right)^2, \tag{6b}$$

$$\gamma_{x\theta} = \Re\frac{\partial u_0}{\partial \theta} + z\Re\frac{\partial \varphi_x}{\partial \theta} - \Re\left(v_0 + z\varphi_\theta\right)\sin\beta + \frac{\partial v_0}{\partial x} + z\frac{\partial \varphi_\theta}{\partial x} + \Re\frac{\partial w_0}{\partial x}\frac{\partial w_0}{\partial \theta}, \tag{6c}$$

$$\gamma_{\theta z} = \varphi_\theta + \Re\frac{\partial w_0}{\partial \theta} - \Re v_0\cos\beta, \tag{6d}$$

$$\gamma_{xz} = \frac{\partial w_0}{\partial x} + \varphi_x, \tag{6e}$$

where $\Re = 1/R$, ε_x and ε_θ stand for principal strains, $\gamma_{x\theta}$, $\gamma_{\theta z}$, and γ_{xz} denote shear strains.

The thermal effect on the FGM truncated conical shell is considered. As a result of the viscous aerodynamic heating on the outside surface of the FGM truncated conical shell, the temperature can be calculated as follow [54]

$$T_c = T_\infty + R_f\frac{\gamma - 1}{2}M_a^2 T_\infty, \tag{7}$$

where T_∞, T_c, R_f and γ are the temperature of the incoming flow, the temperature of the outside surface for the FGM truncated conical shell, the steady-state temperature recovery factor and the specific heat ratio, respectively.

The temperature distribution along the radial direction of the FGM truncated conical shell is regarded as polynomial series [55]

$$T(z) = T_m + (T_c - T_m)\varsigma(z), \tag{8}$$

where the polynomial series $\varsigma(z)$ is shown

$$\varsigma(z)=\frac{1}{C}\left[\left(\frac{2z+h}{2h}\right)-\frac{k_{cm}}{k_m(\eta+1)}\left(\frac{2z+h}{2h}\right)^{(\eta+1)}+\frac{k_{cm}^2}{k_m^2(2\eta+1)}\left(\frac{2z+h}{2h}\right)^{(2\eta+1)}\right.$$
$$\left.-\frac{k_{cm}^3}{k_m^3(3\eta+1)}\left(\frac{2z+h}{2h}\right)^{(3\eta+1)}+\frac{k_{cm}^4}{k_m^4(4\eta+1)}\left(\frac{2z+h}{2h}\right)^{(4\eta+1)}-\frac{k_{cm}^5}{k_m^5(5\eta+1)}\left(\frac{2z+h}{2h}\right)^{(5\eta+1)}\right], \tag{9}$$

with

$$k_{cm}=k_c-k_m, \tag{10}$$

and

$$C=1-\frac{k_{cm}}{(\eta+1)k_m}+\frac{k_{cm}^2}{(2\eta+1)k_m^2}-\frac{k_{cm}^3}{(3\eta+1)k_m^3}+\frac{k_{cm}^4}{(4\eta+1)k_m^4}-\frac{k_{cm}^5}{(5\eta+1)k_m^5}, \tag{11}$$

where k_m and k_c are the thermal conductivities of the metal and ceramic.

The constitutive relations of FGM truncated conical shell with the thermal stress can be yielded as

$$\begin{Bmatrix}\sigma_x\\ \sigma_\theta\\ \sigma_{x\theta}\\ \sigma_{\theta z}\\ \sigma_{xz}\end{Bmatrix}=\begin{bmatrix}Q_{11}&Q_{12}&0&0&0\\ Q_{12}&Q_{22}&0&0&0\\ 0&0&Q_{66}&0&0\\ 0&0&0&Q_{44}&0\\ 0&0&0&0&Q_{55}\end{bmatrix}\left\{\begin{Bmatrix}\varepsilon_x\\ \varepsilon_\theta\\ \gamma_{x\theta}\\ \gamma_{\theta z}\\ \gamma_{xz}\end{Bmatrix}-\begin{Bmatrix}\alpha\\ \alpha\\ 0\\ 0\\ 0\end{Bmatrix}\Delta T\right\}. \tag{12}$$

The temperature variation is regarded as $\Delta T=T(z)-T_0$, and T_0 represents the reference temperature. The stiffness coefficients Q_{ij} are calculated as follow

$$Q_{11}=Q_{22}=\frac{E}{1-\nu^2},\ Q_{12}=\frac{\nu E}{1-\nu^2},\ Q_{44}=Q_{55}=Q_{66}=\frac{E}{2(1+\nu)}. \tag{13}$$

Based on Hamilton's principle, the nonlinear partial differential equations of motion for the truncated FGM conical shell are established as

$$N_{xx,x}+\Re N_{x\theta,\theta}+\Re N_{xx}\sin\beta-\Re N_{\theta\theta}\sin\beta=I_0\ddot{u}_0+I_1\ddot{\varphi}_x, \tag{14a}$$
$$N_{x\theta,x}+\Re N_{\theta\theta,\theta}+2\Re N_{x\theta}\sin\beta+\Re Q_\theta\cos\beta=I_0\ddot{v}_0+I_1\ddot{\varphi}_\theta, \tag{14b}$$
$$\begin{aligned}&Q_{x,x}+\Re Q_{\theta,\theta}+\Re Q_x\sin\beta-\Re N_{\theta\theta}\cos\beta+N_{xx,x}\frac{\partial w_0}{\partial x}+N_{xx}\frac{\partial^2 w_0}{\partial x^2}+\Re N_{xx}\frac{\partial w_0}{\partial x}\sin\beta\\ &+\Re^2 N_{\theta\theta,\theta}\frac{\partial w_0}{\partial\theta}+\Re^2 N_{\theta\theta}\frac{\partial^2 w_0}{\partial\theta^2}+\Re N_{x\theta,\theta}\frac{\partial w_0}{\partial x}+2\Re N_{x\theta,\theta}\frac{\partial^2 w_0}{\partial x\partial\theta}\\ &+\Re N_{x\theta,x}\frac{\partial w_0}{\partial\theta}+P_{\mathrm{a}}-p_1\cos(\Omega t)\frac{\partial^2 w_0}{\partial x^2}-\kappa\dot{w}_0=I_0\ddot{w}_0,\end{aligned} \tag{14c}$$
$$M_{xx,x}+\Re M_{x\theta,\theta}-\Re Q_x+\Re M_{xx}\sin\beta-\Re M_{\theta\theta}\sin\beta=I_1\ddot{u}_0+I_2\ddot{\varphi}_x, \tag{14d}$$
$$M_{x\theta,x}+\Re M_{\theta\theta,\theta}-\Re Q_\theta+2\Re M_{x\theta}\sin\beta=I_1\ddot{v}_0+I_2\ddot{\varphi}_\theta, \tag{14e}$$

where $\Re=1/R$, κ represents damping coefficient of the shell, "$\cdot$" is partial derivative with respect to the time.

All the inertia terms truncated FGM conical shell in the above equations are given

$$I_i=\int_{-\frac{h}{2}}^{\frac{h}{2}}z^i\rho\mathrm{d}z,\ (i=0,\ 1,\ 2). \tag{15}$$

The components of the thermal stress and stress resultants are calculated as

$$\begin{Bmatrix}N_{xx}\\ N_{\theta\theta}\\ N_{x\theta}\end{Bmatrix}=\int_{-\frac{h}{2}}^{\frac{h}{2}}\{[A],[B]\}\begin{Bmatrix}\varepsilon^{(0)}\\ \varepsilon^{(1)}\end{Bmatrix}\mathrm{d}z+\begin{Bmatrix}N_{xx}^T\\ N_{\theta\theta}^T\\ 0\end{Bmatrix}, \tag{16a}$$

$$\begin{Bmatrix} M_{xx} \\ M_{\theta\theta} \\ M_{x\theta} \end{Bmatrix} = \int_{-\frac{h}{2}}^{\frac{h}{2}} \{[B],[D]\} \begin{Bmatrix} \varepsilon^{(0)} \\ \varepsilon^{(1)} \end{Bmatrix} \mathrm{d}z + \begin{Bmatrix} M_{xx}^{T} \\ M_{\theta\theta}^{T} \\ 0 \end{Bmatrix}, \tag{16b}$$

$$\begin{Bmatrix} Q_x \\ Q_\theta \end{Bmatrix} = K \int_{-\frac{h}{2}}^{\frac{h}{2}} [A] \begin{Bmatrix} \gamma_{xz} \\ \gamma_{\theta z} \end{Bmatrix} \mathrm{d}z, \tag{16c}$$

$$\left(\begin{Bmatrix} N_{xx}^{T} \\ N_{\theta\theta}^{T} \\ N_{x\theta}^{T} \end{Bmatrix}, \begin{Bmatrix} M_{xx}^{T} \\ M_{\theta\theta}^{T} \\ M_{x\theta}^{T} \end{Bmatrix} \right) = \int_{z_k}^{z_{k+1}} \begin{bmatrix} Q_{11} & Q_{12} & 0 \\ Q_{12} & Q_{22} & 0 \\ 0 & 0 & Q_{66} \end{bmatrix} \begin{Bmatrix} \alpha_x \\ \alpha_\theta \\ \alpha_{x\theta} \end{Bmatrix} (\Delta T, \Delta T z)\, \mathrm{d}z, \tag{16d}$$

where K is the shear correction coefficient and give it as follows [56]

$$K = \frac{5}{(6-\nu)}. \tag{17}$$

The tensile rigidity A_{ij}, the bending-tensile coupling rigidity B_{ij}, and the bending rigidity D_{ij} of the FGM truncated conical shell can be expressed by

$$\left(A_{ij}, B_{ij}, D_{ij}\right) = \int_{-\frac{h}{2}}^{\frac{h}{2}} Q_{ij} \left(1, z, z^2\right) \mathrm{d}z, \quad (i, j = 1, 2, 6), \tag{18a}$$

$$A_{ij} = \int_{-\frac{h}{2}}^{\frac{h}{2}} Q_{ij} \mathrm{d}z, \quad (i, j = 4, 5). \tag{18b}$$

Using the aforementioned equations, the nonlinear equations of motion in form of generalized displacements for the FGM truncated conical shell are given in the "Appendix A."

The boundary conditions of the FGM truncated conical shell are considered as the simply supported at the two ends

$$x = 0 \text{ and } x = L : w_0 = \ v_0 = N_x = M_x = M_{x\theta} = 0. \tag{19}$$

The displacements u_0, v_0, w_0, φ_x and φ_θ of the FGM truncated conical shell, which satisfy the boundary conditions, are represented in the form of the double Fourier sine series

$$u_0 = \sum_{m=1}^{M} \sum_{n=1}^{N} u_{mn}(t) \cos\left(\frac{m\pi x}{L}\right) \cos(n\theta), \tag{20a}$$

$$v_0 = \sum_{m=1}^{M} \sum_{n=1}^{N} v_{mn}(t) \sin\left(\frac{m\pi x}{L}\right) \sin(n\theta), \tag{20b}$$

$$w_0 = \sum_{n=1}^{M} \sum_{m=1}^{N} W_{mn}(t) \sin\left(\frac{m\pi x}{L}\right) \cos(n\theta), \tag{20c}$$

$$\varphi_x = \sum_{m=1}^{M} \sum_{n=1}^{N} \varphi_{xmn}(t) \cos\left(\frac{m\pi x}{L}\right) \sin(n\theta), \tag{20d}$$

$$\varphi_\theta = \sum_{m=1}^{M} \sum_{n=1}^{N} \varphi_{\theta mn}(t) \sin\left(\frac{m\pi x}{L}\right) \sin(n\theta), \tag{20e}$$

where $u_{mn}(t)$, $v_{mn}(t)$, $W_{mn}(t)$, $\varphi_{xmn}(t)$ and $\varphi_{\theta mn}(t)$ are the time-varying terms, m and n are the generatrix half waves number and the circumferential waves number.

Based on the study results of Noseir [57] and Bhimaraddi [58], the influences of the inertia terms in rotation and in-plane on nonlinear vibrations of FGM truncated conical shell are very small comparing to radial inertia term which given in Eq. (18). Thus, the inertia terms of u_0, v_0, φ_x and φ_θ can be omitted. Thus, the first two modes of transverse displacement w are very important. Substituting the double Fourier series of Eq. (20) into Eqs. (A1), (A2), (A4) and (A5), Galerkin integration procedure is employed to acquire four constant

coefficients of the coupled algebraic equations. Then, the displacements u_0, v_0, φ_x and φ_θ with respect to the displacement w_0 can be derived. Therefore, substituting the expressions about u_0, v_0, φ_x and φ_θ into the ordinary differential equation obtained by Eq. (A3), the nonlinear ordinary differential equations of motion for the FGM truncated conical shell are obtained

$$\ddot{W}_{11} + \mu_1 \dot{W}_{11} + \omega_1^2 W_{11} + \zeta_{11} W_{11}^3 + \zeta_{12} W_{11}^2 W_{12} + \zeta_{13} W_{11} W_{12}^2 + \zeta_{14} W_{12}^3 + \zeta_{15} W_{11} (p_1 \cos \Omega t) = 0, \tag{21a}$$

$$\ddot{W}_{12} + \mu_2 \dot{W}_{12} + \omega_2^2 W_{12} + \zeta_{21} W_{12}^3 + \zeta_{22} W_{11}^2 W_{12} + \zeta_{23} W_{11} W_{12}^2 + \zeta_{24} W_{12}^3 + \zeta_{25} W_{11} (p_1 \cos \Omega t) = 0, \tag{21b}$$

In order to get the dimensionless equations of the FGM truncated conical shell, the following transformation of the variables and parameters are introduced

$$\begin{aligned} &\tau = \omega_1 t,\ W_{11} = q_1 h,\ W_{12} = q_2 h,\ \bar{\Omega} = \frac{\Omega}{\omega_1},\ \bar{\mu}_1 = \frac{\mu_1}{\omega_1},\ \bar{\mu}_2 = \frac{\mu_2}{\omega_1}, \\ &\bar{\omega}_1 = \frac{\omega_1}{\omega_1},\ \bar{\omega}_2 = \frac{\omega_2}{\omega_1},\ \bar{p}_1 = \frac{p_1}{\omega_1^2},\ \bar{\zeta}_{ij} = \frac{\zeta_{ij} h^2}{\omega_1^2},\ (i = 1,\ 2,\ j = 1,\ 2,\ 3,\ 4). \end{aligned} \tag{22}$$

Thus, the dimensionless equation of the FGM truncated conical shell can be rewritten as

$$\ddot{q}_1 + \bar{\mu}_1 \dot{q}_1 + \bar{\omega}_1^2 q_1 + \bar{\zeta}_{11} q_1^3 + \bar{\zeta}_{12} q_1^2 q_2 + \bar{\zeta}_{13} q_1 q_2^2 + \bar{\zeta}_{14} q_2^3 + \bar{\zeta}_{15} q_1 \left(\bar{p}_1 \cos \bar{\Omega} \tau\right) = 0, \tag{23a}$$

$$\ddot{q}_2 + \bar{\mu}_2 \dot{q}_2 + \bar{\omega}_2^2 q_2 + \bar{\zeta}_{21} q_1^3 + \bar{\zeta}_{22} q_1^2 q_2 + \bar{\zeta}_{23} q_1 q_2^2 + \bar{\zeta}_{24} q_2^3 + \bar{\zeta}_{25} q_1 \left(\bar{p}_1 \cos \bar{\Omega} \tau\right) = 0, \tag{23b}$$

where "$\cdot$" stands for the derivative with respect to the dimensionless time τ.

3 Perturbation analysis

By using the scale method [59], a perturbation analysis is carried out in following study. A small perturbation parameter ε is introduced to characterize the amplitude of the radial displacement, the loading and the damping of the FGM truncated conical shell

$$q_i = \varepsilon w_i,\ \tilde{\mu}_i = \varepsilon^2 \bar{\mu}_i,\ \tilde{p} = \varepsilon^2 \bar{p},\ (i = 1,\ 2). \tag{24}$$

Substituting Eq. (24) into Eq. (23), the dimensionless system is obtained as follows. For simplicity, the overbars are omitted in the following equations

$$\begin{aligned} &\ddot{w}_1 + \varepsilon \mu_1 \dot{w}_1 + \omega_1^2 w_1 + \varepsilon \zeta_{11} w_1^3 + \varepsilon \zeta_{12} w_1^2 w_2 + \varepsilon \zeta_{13} w_1 w_2^2 + \varepsilon \zeta_{14} w_2^3 \\ &\quad + \varepsilon \zeta_{15} w_1 (p_1 \cos \Omega t) = 0, \end{aligned} \tag{25a}$$

$$\begin{aligned} &\ddot{w}_2 + \varepsilon \mu_2 \dot{w}_2 + \omega_2^2 w_2 + \varepsilon \zeta_{21} w_2^3 + \varepsilon \zeta_{22} w_1^2 w_2 + \varepsilon \zeta_{23} w_1 w_2^2 + \varepsilon \zeta_{24} w_2^3 \\ &\quad + \varepsilon \zeta_{25} w_1 (p_1 \cos \Omega t) = 0. \end{aligned} \tag{25b}$$

For utilizing the multiple scales method, the approximate solutions of Eq. (25) are assumed as follows

$$w_n(\tau,\ \varepsilon) = x_{n0}(T_0, T_1) + \varepsilon x_{n1}(T_0, T_1) + \cdots,\ (n = 1,\ 2), \tag{26}$$

where $T_0 = \tau$, $T_1 = \varepsilon \tau$.

Then, one obtains the following differential operators

$$\frac{\mathrm{d}}{\mathrm{d}\tau} = \frac{\partial}{\partial T_0} \frac{\partial T_0}{\partial \tau} + \frac{\partial}{\partial T_1} \frac{\partial T_1}{\partial \tau} + \cdots = D_0 + \varepsilon D_1 + \cdots, \tag{27a}$$

$$\frac{\mathrm{d}^2}{\mathrm{d}\tau^2} = (D_0 + \varepsilon D_1 \cdots)^2 = D_0^2 + 2\varepsilon D_0 D_1 + \cdots, \tag{27b}$$

where $D_k = \frac{\partial}{\partial T_k}$, $(k = 0,\ 1)$.

The following analyses are focused on the case of 1:2 internal resonant and 1/2 subharmonic resonant relations. Therefore, the resonant relations can be proved as

$$2\omega_1 = \Omega - \varepsilon\sigma_1, \omega_2 = \Omega - \varepsilon\sigma_2, \Omega = 2, \tag{28}$$

where σ_1 and σ_2 are the detuning parameters.

Substituting Eqs. (26)–(28) into Eq. (25) and equating the coefficients of the same power of ε yield the following equations

Order ε^0

$$D_0^2 x_{10} + x_{10} = 0, \tag{29a}$$

$$D_0^2 x_{20} + x_{20} = 0, \tag{29b}$$

Order ε^1

$$\begin{aligned} D_0^2 x_{11} + \frac{x_{11}}{4} = &-2D_0 D_1 x_{10} - \mu_1 D_0 x_{10} + \frac{\sigma_1}{2} x_{10} - \zeta_{11} x_{10}^3 - \zeta_{12} x_{10}^2 x_{20} \\ &-\zeta_{13} x_{10} x_{20}^2 - \zeta_{14} x_{20}^3 - \zeta_{15} x_{10} p_1 \cos(\tau), \end{aligned} \tag{30a}$$

$$\begin{aligned} D_0^2 x_{21} + x_{21} = &-2D_0 D_1 x_{20} - \mu_2 D_0 x_{20} + 2\sigma_2 x_{20} - \zeta_{21} x_{10}^3 - \zeta_{22} x_{10}^2 x_{20} \\ &-\zeta_{23} x_{10} x_{20}^2 - \zeta_{24} x_{20}^3 - \zeta_{25} x_{20} p_1 \cos(\tau). \end{aligned} \tag{30b}$$

The solution of Eq. (29) is represented in the complex form

$$x_{10} = A_1(T_1) \mathrm{e}^{\frac{i}{2}T_0} + \bar{A}_1(T_1) \mathrm{e}^{-\frac{i}{2}T_0}, \tag{31a}$$

$$x_{20} = A_2(T_1) \mathrm{e}^{\frac{i}{2}T_0} + \bar{A}_2(T_1) \mathrm{e}^{-\frac{i}{2}T_0}, \tag{31b}$$

where $\bar{A}_1$ and $\bar{A}_2$ are the complex conjugate parts of A_1 and A_2, respectively.

Substituting Eq. (31) into Eq. (30), one yields

$$\begin{aligned} D_0^2 x_{11} + \frac{x_{11}}{4} = &\left(-iD_1 A_1 - \frac{\mu_1 i}{2} A_1 + \frac{\sigma_1}{2} A_1 - 3\zeta_{11} A_1^2 \bar{A}_1 - 2\zeta_{12} A_1 \bar{A}_1 A_2 \right. \\ &\left. -\frac{1}{2}\zeta_{15} p_1 \bar{A}_1 \right) \mathrm{e}^{\frac{i}{2}T_0} + CC + NST, \end{aligned} \tag{32a}$$

$$\begin{aligned} D_0^2 x_{21} + x_{21} = &\left(-2iD_1 A_2 - \mu_2 i A_2 + 2\sigma_2 A_2 - 2\zeta_{22} A_1 \bar{A}_1 A_2 - 3\zeta_{24} A_2^2 \bar{A}_2 \right. \\ &\left. -\frac{1}{2}\zeta_{25} p_1 \bar{A}_2 \right) \mathrm{e}^{iT_0} + CC + NST, \end{aligned} \tag{32b}$$

where CC stand for the complex conjugate terms of the preceding parts and NST stand for the parts which cannot produce the secular terms.

The amplitude functions can be written in polar form as

$$A_1 = \frac{1}{2} a_1 \mathrm{e}^{i\varphi_1}, A_2 = \frac{1}{2} a_2 \mathrm{e}^{i\varphi_2}. \tag{33}$$

Substituting Eq. (33) into the parts that producing the secular terms of Eq. (32), the averaged equations in polar form are yielded by separating the real and imaginary parts

$$\frac{\mathrm{d}a_1}{\mathrm{d}T_1} = -\frac{\mu_1 a_1}{2} - \frac{\zeta_{15} p_1 a_1}{2} \sin(2\varphi_1), \tag{34a}$$

$$a_1 \frac{\mathrm{d}\varphi_1}{\mathrm{d}T_1} = -\frac{\sigma_1 a_1}{2} - \frac{\zeta_{15} p_1 a_1}{2} \cos(2\varphi_1) + \frac{3\zeta_{11} a_1^3}{4} + + \frac{\zeta_{13} a_1 a_2^2}{2}, \tag{34b}$$

$$\frac{\mathrm{d}a_2}{\mathrm{d}T_1} = -\frac{\mu_2 a_2}{2} - \frac{\zeta_{25} p_1 a_2}{4} \sin(2\varphi_2), \tag{34c}$$

$$a_2 \frac{\mathrm{d}\varphi_2}{\mathrm{d}T_1} = -\frac{\sigma_2 a_2}{2} - \frac{\zeta_{25} p_1 a_2}{2} \cos(2\varphi_2) - \frac{3\zeta_{21} a_2^3}{8} + \frac{\zeta_{23} a_1^2 a_2}{4}. \tag{34d}$$

Table 1 The material properties of SUS304, SI_3N_4 and ZrO_2 are given

	SUS304			SI_3N_4			ZrO_2		
	E (Pa)	ρ (kg/m^3)	α (1/K)	E (Pa)	ρ (kg/m^3)	α (1/K)	E (Pa)	ρ (kg/m^3)	α (1/K)
P_{-1}	0	0	0	0	0	0	0	0	0
P_0	201.04e−9	8166	12.33e−6	348.43e−9	2370	5.872e−6	244.27e9	3000	12.766e−6
P_1	3.079e−4	0	8.08e−4	− 3.07e−4	0	9.09e−4	− 1.371e−4	0	− 1.491e−3
P_2	− 6.53e−7	0	0	2.16e−7	0	0	1.214e−6	0	1.006e−5
P_3	0	0	0	− 8.95e−11	0	0	− 3.681e−10	0	− 6.778e−11

Table 2 Comparison of the dimensionless transverse amplitudes of the FGM truncated conical shell at the point (3L/4, 0, 0) for first mode, first two modes and first three modes is given

p_1	First mode	First two modes	First three modes
60	2.9566	3.1742	3.1733
70	6.3252	6.8563	6.8552
80	6.5461	6.9806	6.9785

The amplitude functions are also rewritten in the Cartesian form, as following

$$A_1 = x_1 + ix_2,\ A_2 = x_3 + ix_4. \tag{35a}$$

Substituting Eq. (35) into the parts that producing the secular terms of Eq. (32) and separating the real and imaginary parts, the four-dimensional averaged equations in the form of Cartesian can be obtained as

$$\frac{\mathrm{d}x_1}{\mathrm{d}T_1} = \frac{\sigma_1 x_2}{2} - \frac{\mu_1 x_1}{2} - \frac{\zeta_{15} p_1 x_2}{4} - 3\zeta_{11}x_2^3 - 3\zeta_{11}x_1^2 x_2 - 2\zeta_{13}x_2 x_3^2 - 2\zeta_{13}x_2 x_4^2, \tag{36a}$$

$$\frac{\mathrm{d}x_2}{\mathrm{d}T_1} = -\frac{\sigma_1 x_1}{2} - \frac{\mu_1 x_2}{2} - \frac{\zeta_{15} p_1 x_1}{4} + 3\zeta_{11}x_1^3 + 3\zeta_{11}x_1 x_2^2 + 2\zeta_{13}x_1 x_3^2 + 2\zeta_{13}x_1 x_4^2, \tag{36b}$$

$$\frac{\mathrm{d}x_3}{\mathrm{d}T_1} = \sigma_2 x_4 - \frac{\mu_2 x_3}{2} - \frac{\zeta_{25} p_1 x_4}{4} - \frac{3\zeta_{21}x_4^3}{2} - \frac{3\zeta_{21}x_3^2 x_4}{2} - \zeta_{23}x_1^2 x_4 - \zeta_{23}x_2^2 x_4, \tag{36c}$$

$$\frac{\mathrm{d}x_4}{\mathrm{d}T_1} = -\sigma_2 x_3 - \frac{\mu_2 x_4}{2} - \frac{\zeta_{25} p_1 x_3}{4} + \frac{3\zeta_{21}x_3^3}{2} + \frac{3\zeta_{21}x_3 x_4^2}{2} + \zeta_{23}x_1^2 x_3 + \zeta_{23}x_2^2 x_3. \tag{36d}$$

4 Frequency responses

In this section, a FGM (SUS304/SI_3N_4) truncated conical shell are considered, the smaller radius at middle surface $r_1 = 0.8$ m, semi-vertex angle $\beta = 30°$ and thickness $h = 0.002$ m. The mass densities, Young's modulus and coefficients of thermal expansion of SUS304 and SI_3N_4 are given in Table 1. The airflow characteristics are provided as following: $\alpha_\infty = 213.36$ m/s, $\gamma_\alpha = 1.4$ and $T_\infty = 233.26$ K. In Fig. 4, when the ratio of the length to the smaller radius is $L/r_1 = 3.76$, it is found that the natural frequency $\omega_2 = 2\omega_1$, then, $\bar{\omega}_2 = \omega_2/\omega_1 = 2$. When the in-plane load frequency is close to $2\omega_1$, there will be the case of 1:2 internal resonant and 1/2 subharmonic resonant relations.

Firstly, the mode convergence is studied. The condition which the 1:2 internal resonance occurs of the FGM truncated conical shell is considered. The dimensionless transverse amplitudes of the FGM truncated conical shell at the point ($3L/4$, 0, 0) with first mode (1, 1), first two modes (1, 1) and (1, 2), first three modes (1, 1), (1, 2) and (2, 1) are calculated in Table 1, respectively, when exponent of volume fraction for the ceramic $\eta = 5$ and Mach number $M_a = 3$. It can be seen that the amplitudes of the FGM truncated conical shell with 1:2 internal resonance obtained with the first two modes and the first three modes are nearly the same, and a further increase in the number of components does not greatly influence the results.

To evaluate the developed program and present formulation, the dimensionless natural frequencies ($\Omega_n = \omega_n R\sqrt{\left(1-\nu^2\right)\rho/E}$) are calculated and are compared to those of Liew [60], Kerboua [61] and Najafov [62] for a pure metal conical shell in Table 3. The geometry relations of the pure metal truncated conical shell

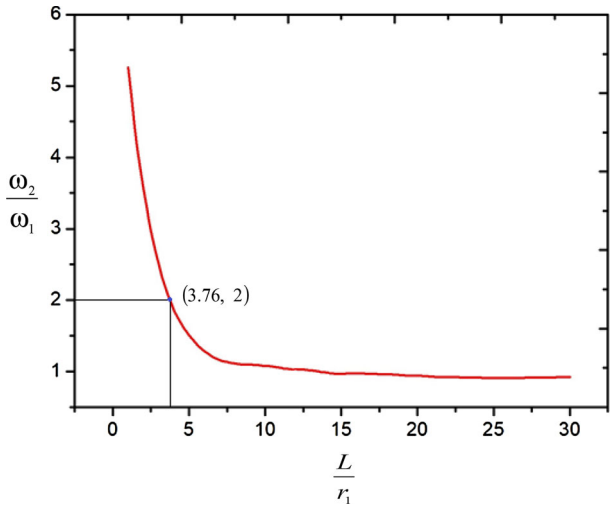

Fig. 4 The curve of the ratio of the first two order natural frequencies ω_2/ω_1 versus the ratio of length to top radius L/r_1 is obtained

Table 3 The comparison of dimensionless natural frequency $\left(\Omega_n = \omega_n R\,(L)\sqrt{\left(1-\nu^2\right)\rho/E}\right)$ for truncated pure metal conical shell with Liew [50], Kerboua [51] and Najafov [52] is obtained

n	Liew et al. [50]	Kerboua et al. [51]	Najafov et al. [52]	Present study
2	0.7904	0.7909	0.7943	0.7922
3	0.7274	0.7282	0.7085	0.7089
4	0.6339	0.6349	0.6199	0.6357

Table 4 The comparison of natural frequencies with Pradhan et al. [53] and Shen [54] for thin FGM (SUS304/ZrO_2) cylindrical shell is obtained

Frequencies (Hz)	Pradhan et al. [65]	Shen [27]	Present study
(1, 3)	4.67	4.911	4.915
(1, 4)	7.91	7.883	7.886
(1, 5)	12.18	12.179	12.183
(1, 6)	18.17	17.502	17.507

Table 5 Comparison of the dimensionless central moments $\bar{M}_{xx} = M_{xx}/\left(q_0 a^2\right)$ and $\bar{M}_{yy} = M_{yy}/\left(q_0 a^2\right)$ for $\eta = 0.5$ and 1.0 is given

η	$\bar{M}_{xx}$		$\bar{M}_{yy}$	
	Ref. [29]	Present	Ref. [29]	Present
0.5	0.01774	0.01742	0.01769	0.01792
1.0	0.01776	0.01801	0.01794	0.01813

are $R/h = 100$, $\beta = \pi/6$ and $L = 0.25R\sin\beta$. As expected, for the pure metal truncated conical shell, the present results are in good agreement with that in the literatures. Furthermore, the natural frequencies are compared with Pradhan et al. [62] and Shen [63] for the FGM (SUS304/ZrO_2) cylindrical shell, as shown in Table 4. The geometric parameters of the cylindrical shell are given: $h = 0.002$ m, $R = 1$ m and $L = 20$ m. The material properties of the FGM (SUS304/ZrO2) are shown in Table 1. It is illuminated that the present results are agree well with the existing results.

In addition, the validation of the present method has been done by comparing the dimensionless central moments of FGM plate in Table 5 with the value obtained by using the method which is provided by Ref. [51]. The Ti–6Al–4V/Al_2O_3 FGM plate has the length $a = 0.2$ m, the width $b = 0.5$ m and the thickness $h = 0.002$ m. One can note that excellent agreement is reached.

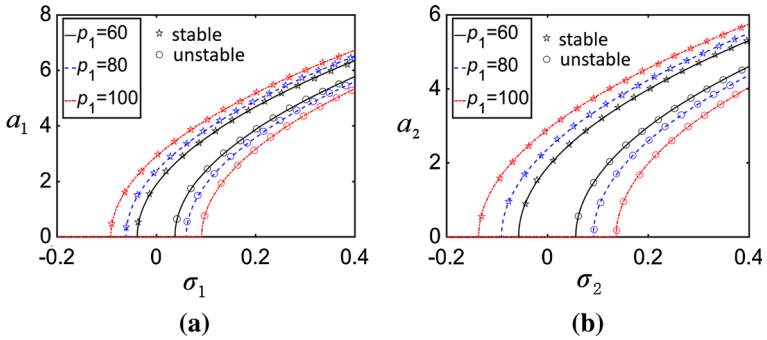

Fig. 5 The frequency–amplitude response curves of the FGM conical truncated shell with different in-plane loads p_1 are obtained when $\eta = 5$ and $M_a = 2$, **a** the first-order mode, **b** the second-order mode

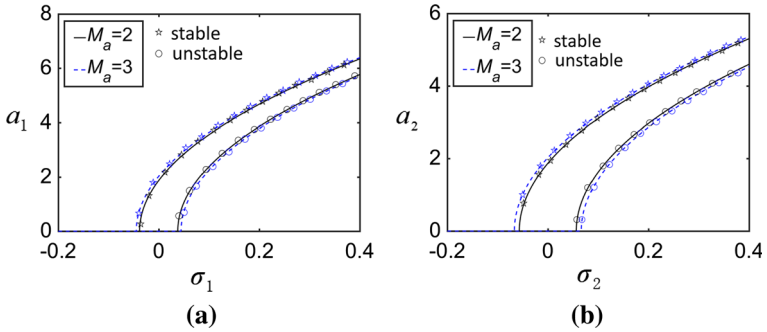

Fig. 6 The frequency–amplitude response curves of the truncated FGM conical shell with different Mach numbers M_a are obtained when $\eta = 5$ and $p_1 = 60$

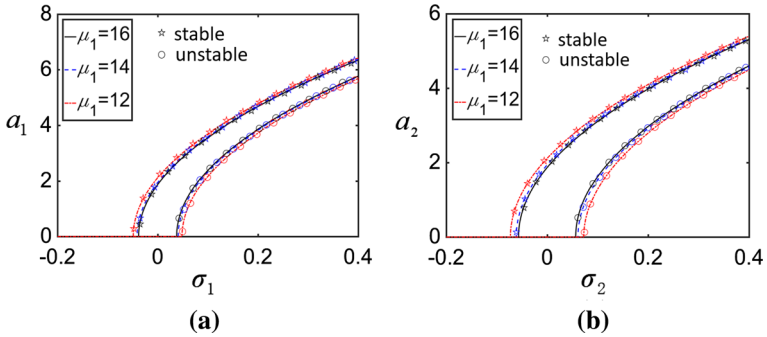

Fig. 7 The frequency–amplitude response curves of the truncated FGM conical shell with different damping coefficient μ_1 are obtained when $\eta = 5$ and $p_1 = 60$

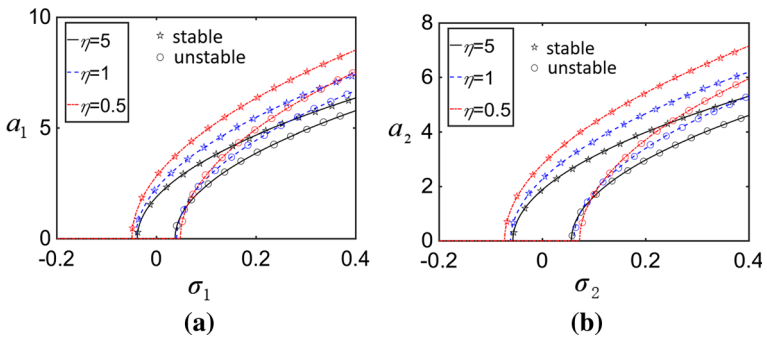

Fig. 8 The frequency–amplitude response curves of the FGM truncated conical shell with different exponents of volume fraction η are obtained when $M_a = 2$ and $p_1 = 60$

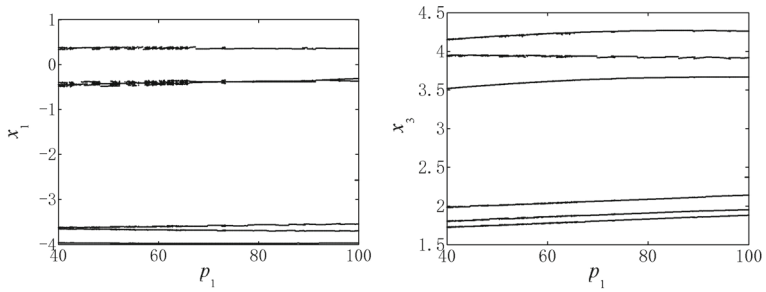

Fig. 9 The bifurcation diagram of the truncated FGM conical shell for the in-plane load p_1 is obtained when the exponents of volume fraction for the ceramic $\eta = 0.5$ and Mach number $M_a = 2$, **a** bifurcation diagram of the first-order mode, **b** bifurcation diagram of the second-order mode

In the following studies, the numerical calculations are used to investigate the nonlinear dynamics of the FGM truncated conical shell subject to aerodynamics and in-plane load. Based on the averaged equation (34), amplitude–frequency responses of the FGM truncated conical shell can be investigated. The left parts of the averaged equation (34) are proposed to zero. Then, using Maple program, the amplitude–frequency and amplitude–force response curves of the FGM truncated conical shell are plotted. By inspecting the maximum real part of the Jacobian matrix of the averaged equation (34), the stabilities of the solutions can be revealed.

Figure 5 depicts the frequency–amplitude response curves of the FGM conical truncated shell with different in-plane loads p_1. Mach number is selected as 2, and the value of the volume fraction index is 5. Figure 5a and b is the frequency–amplitude response curves of the first-order mode and the second-order mode of the FGM truncated conical shell, respectively. The full line, the dash line and the dot dash line represent the frequency amplitude-response curves with different in-plane loads which are chosen as 60, 80 and 100, respectively. The star represents the stable solutions, and the circle represents the unstable solutions. The upper branch of the frequency–amplitude response curves of the FGM conical truncated shell is stable and the lower branch is unstable. By comparing the three lines which in Fig. 5a and b, it is illustrated that there are hardening-spring characteristics for the two modes of the FGM truncated conical shell. The region of two curves becomes wider when in-plane load increasing for the FGM truncated conical shell. It is observed that the nonlinear resonance characteristics become stronger and amplitudes of the two modes are getting larger when the in-plane excitation increasing. Figure 6 illustrates the effect of Mach number of the FGM truncated conical shell on the frequency–amplitude characteristics. No matter what Mach number is 2 or 3, there are hardening-spring characteristics for the two modes of the FGM truncated conical shell. The region of two curves for $M_a = 3$ is little wider than that for $M_a = 2$. It is due to that with the increase of Mach number, the effects of the aerodynamic heating and the aerodynamic force of the FGM truncated conical shell becoming powerful. Figure 7 plots amplitude–response curves with different damping coefficients μ_1 when $M_a = 2$ and $p_1 = 60$. It is shown that with the increase of the damping coefficients, the nonlinear resonance characteristics are getting weaker and amplitudes of two modes become smaller. Figure 8 illustrates the influence of the volume fraction index of the FGM truncated conical shell on the frequency–amplitude responses. It is shown that with the decrease of the volume fraction index, the nonlinear resonance characteristics are stronger and the amplitudes become larger for the two modes of the FGM truncated conical shell.

5 Periodic and chaotic motions

Based on Eq. (36), the chaotic and periodic motions of the truncated FGM conical shell are investigated. The fourth-order varied-step Runge-Kutta algorithm through the MATLAB software is used to explore the existence of the chaotic and periodic motions for the truncated FGM conical shell. The bifurcation diagrams, time phase portraits, Poincare maps and history diagrams can be plotted to reveal the influences of in-plane load, Mach number, exponent of volume fraction and damping coefficient on the nonlinear vibrations and chaos of the truncated FGM conical shell.

Figure 9 plots the bifurcation diagrams of the first-order and second-order modes of the truncated FGM conical shell versus in-plane load when p_1 increases from 60 to 100. Mach number is $M_a = 2$, and the exponents of the volume fraction for the ceramic is $\eta = 0.5$. It can be observed that there is only the periodic

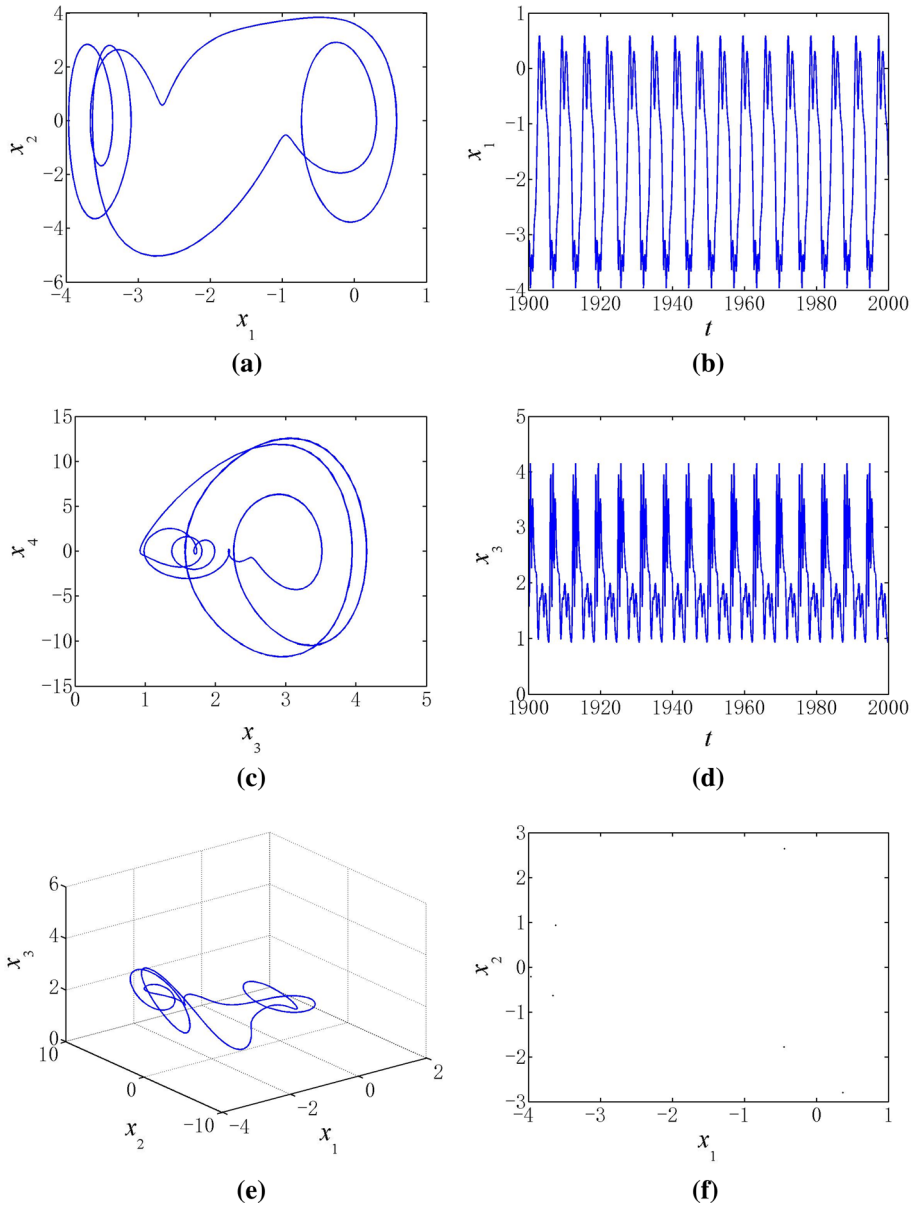

Fig. 10 The period motion of the truncated FGM conical shell exists when $\eta = 0.5$, $M_a = 2$ and $p_1 = 60$, **a** the phase portrait on the plane $(x_1\ ,\ x_2)$, **b** the time history on the plane$(\tau\ ,\ x_1)$, **c** the phase portrait on the plane $(x_3\ ,\ x_4)$, **d** the time history on the plane $(\tau\ ,\ x_3)$, (e) the three-dimensional phase portrait in the space $(x_1\ ,\ x_2, x_3)$, **f** the poincare map on the plane $(x_1\ ,\ x_2)$

motion for the truncated FGM conical shell. It is due to the fact that the volume index is lower, the volume fraction of ceramic is higher, the stiffness of the FGM truncated conical shell is larger. Figure 10 is the motion responses of the truncated FGM conical shell when in-plane load is 60. The motion responses include the following parts, (a) phase portrait on the plane $(x_1\ ,\ x_2)$, (b) time history on the plane $(\tau\ ,\ x_1)$, (c) phase portrait on the plane $(x_3\ ,\ x_4)$, (d) time history on the plane $(\tau\ ,\ x_3)$, (e) three-dimensional phase portrait in space $(x_1\ ,\ x_2, x_3)$, (f) Poincare map on the plane $(x_1\ ,\ x_2)$.

Figure 11 illustrates the bifurcation diagrams of the nonlinear vibrations of the truncated FGM conical shell versus in-plane load when p_1 increases from 60 to 100. The exponent of volume fractions for ceramic is $\eta = 5$ and Mach number is $M_a = 2$, respectively. It is illuminated that the motion of the truncated FGM conical shell is: the periodic motion $\rightarrow$ the quasi-period motion $\rightarrow$ the chaotic motion. A multiple periodic bifurcation exists in the periodic region when p_1 increases from 65 to 78. Figures 12, 13, 14, 15 and 16 prove the different motion responses of the truncated FGM conical shell when in-plane loads are chosen as different

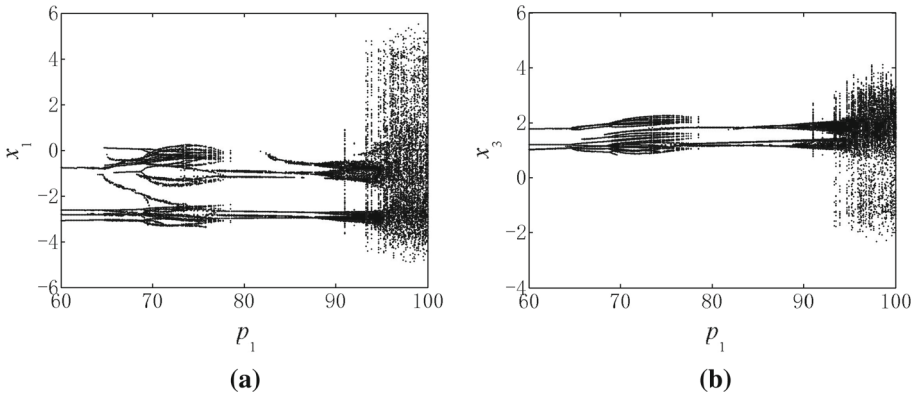

Fig. 11 The bifurcation diagram of the truncated FGM conical shell for the in-plane load p_1 is obtained when the exponents of volume fraction for the ceramic $\eta = 5$ and Mach number $M_a = 2$

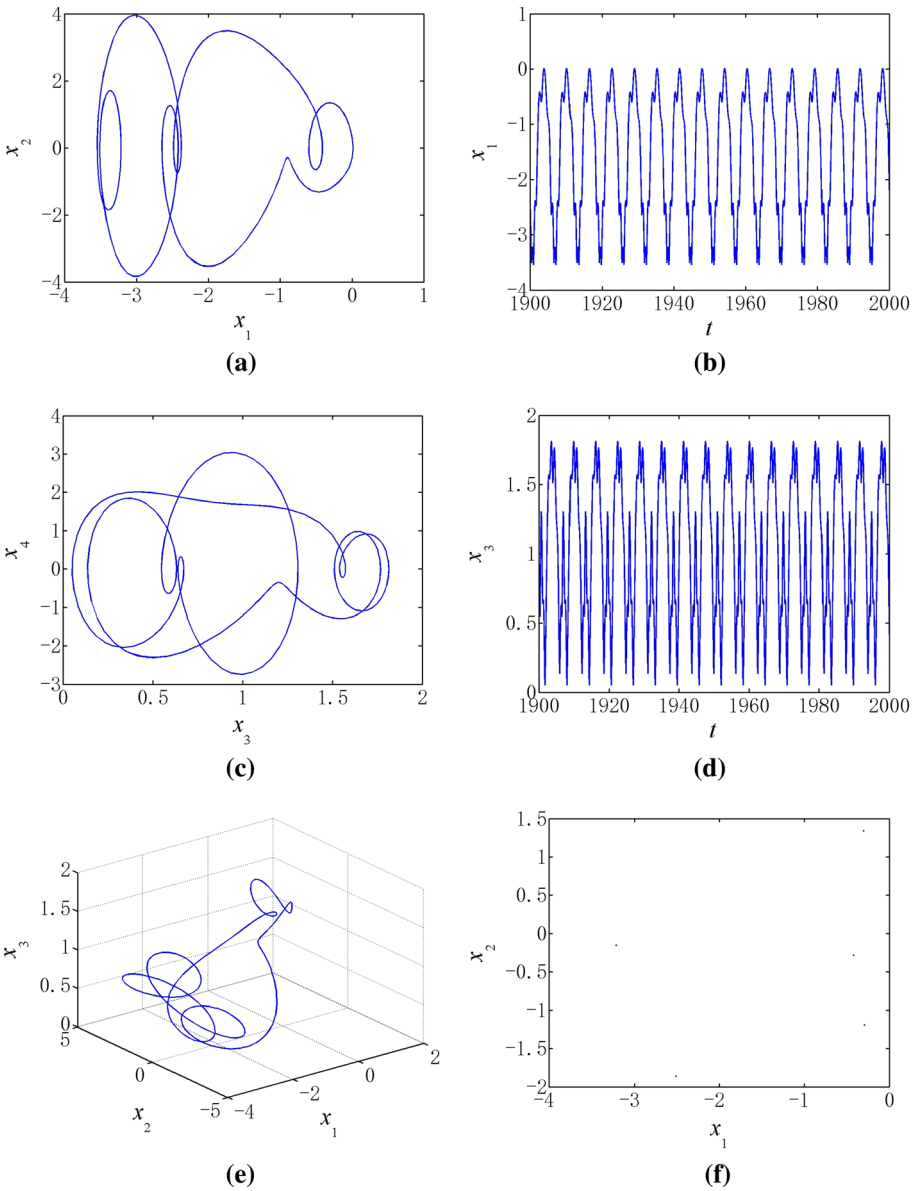

Fig. 12 The period motion of the FGM truncated conical shell is given when $\eta = 5$, $M_a = 2$ and $p_1 = 60$

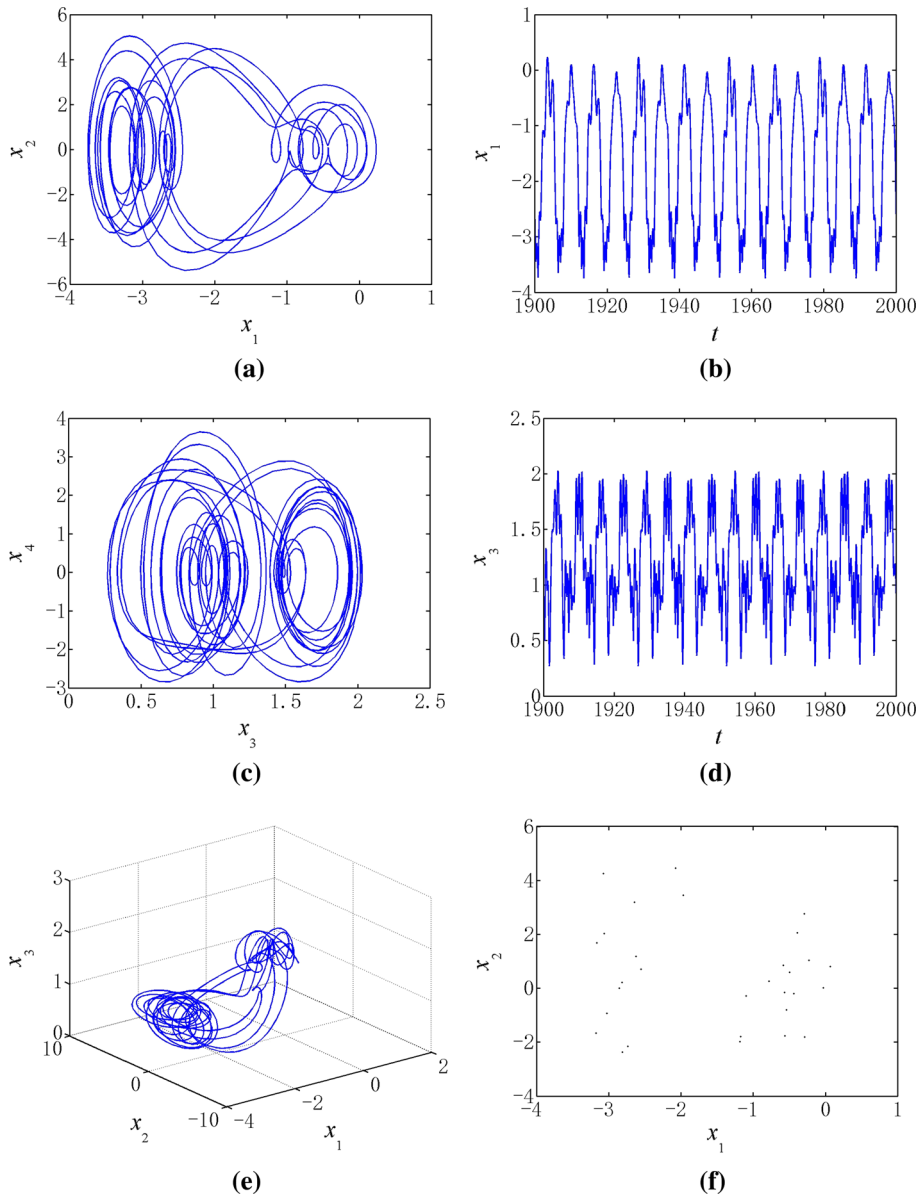

Fig. 13 The period motion of the FGM truncated conical shell is given when $\eta = 5$, $M_a = 2$ and $p_1 = 75$

values. Figures 12, 13 and 14 are the periodic motions of the FGM truncated conical shell when in-plane load are given as $p_1 = 60$, $p_1 = 75$ and $p_1 = 80$, respectively. Figure 13 is the motion response when the multiple periodic bifurcation exists. Figure 15 depicts quasi-period motion of the FGM truncated conical shell when $p_1 = 92$. Figure 16 indicates the chaotic motion of the FGM truncated conical shell when the in-plane load is selected as 100.

Figure 17 illustrates the change of the motion responses of the truncated FGM conical shell from periodic motion to chaotic motion. The exponent of the volume fraction for the ceramic is 5 and Mach number is 3. It is shown that when in-plane load increases to 70, the motion of the FGM truncated conical shell changes from periodic motion to quasi-period motion. Then, there is chaotic motion existing when the in-plane load increases to 78. Figures 18, 19 and 20 depict the periodic motion ($p_1 = 60$), quasi-period motion ($p_1 = 75$) and chaotic motion ($p_1 = 100$), respectively, that are corresponding to the motion responses given in Fig. 17. Comparing these graphs with Figs. 11, 12, 13, 14, 15 and 16, it is found that with the increase of Mach number, chaotic motion and quasi-period motion occur in advance. The amplitude when Mach number is $M_a = 3$ is greater than that in the case of $M_a = 2$. It is because of that when Mach number increases, the aerodynamic

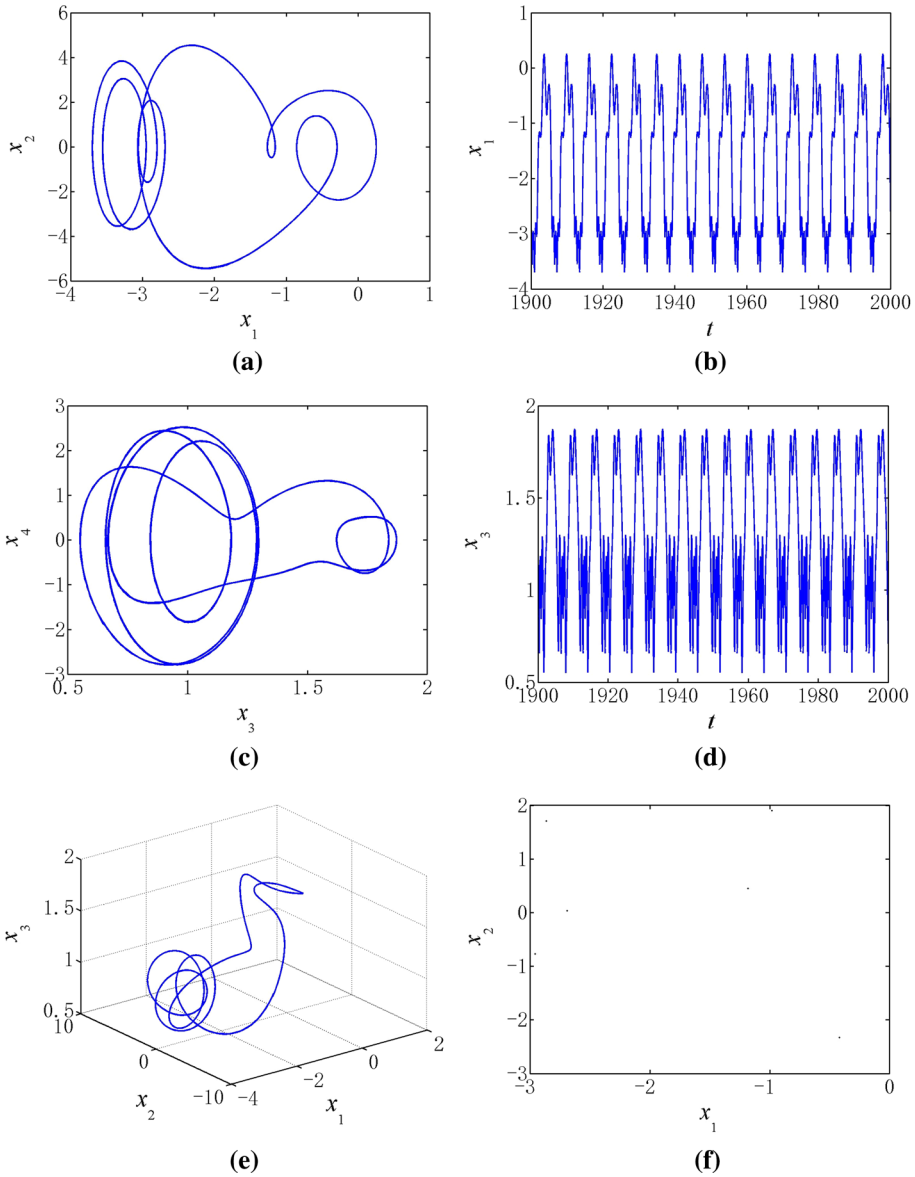

Fig. 14 The period motion of the FGM truncated conical shell is given $\eta = 5$, $M_a = 2$ and $p_1 = 80$

heating creates higher temperature, and thus, the stiffness of the FGM truncated conical shell decreases. At the same time, the influence of the aerodynamic force on the nonlinear vibrations of the FGM truncated conical shell is greater.

The case of the exponent of the volume fraction $\eta = 10$ and Mach number $M_a = 2$ is considered. Figure 21 plots bifurcation diagram of amplitude for the FGM truncated conical shell versus in-plane load when p_1 increases from 40 to 100. The motion responses of the truncated FGM conical shell are given as: periodic motion → quasi-period motion → periodic motion → quasi-period motion → chaotic motion. Figures 22, 23, 24, 25 and 26 depict the different motion responses when the in-plane excitation is chosen as different parameters for the FGM truncated conical shell. Figures 22 and 24 represents the periodic motion of the FGM truncated conical shell, Figs. 23 and 25 indicates the quasi-period motion, Fig. 26 depicts the chaotic motion. By comparing Figs. 9, 17 and 21, it is shown that the chaotic motion yields earlier when the exponent of the volume fraction increases.

Figure 27 depicts the bifurcation diagram of the FGM truncated conical shell for the damping coefficient μ_1 is obtained when the exponents of volume fraction for the ceramic $\eta = 5$, the in-plane load $p_1 = 100$ and

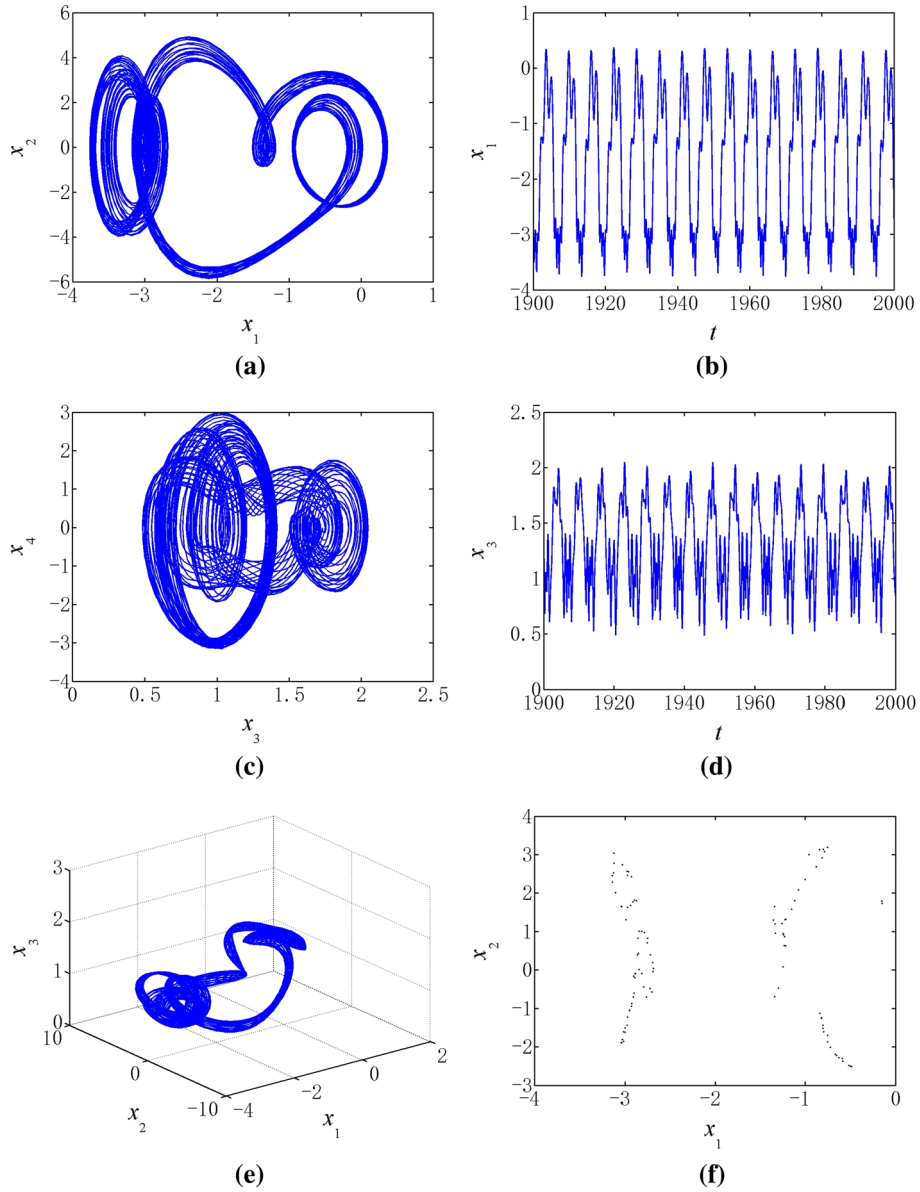

Fig. 15 The quasi-period motion of the FGM truncated conical shell is given when $\eta = 5$, $M_a = 2$ and $p_1 = 92$

Mach number $M_a = 3$. It can be observed that the motions of the FGM truncated conical shell are as follows: chaotic motion → quasi-period motion → chaotic motion → periodic motion. Figure 28 depicts the chaotic motion of the FGM truncated conical shell; Figs. 29 and 31 represents the periodic motion; Fig. 30 indicates the quasi-period motion.

6 Conclusions

In this paper, the nonlinear internal resonance behaviors of a simply supported FGM truncated conical shell with 1:2 internal resonance are investigated. According to a power-law distribution, the material properties are assumed to be modified along the thickness direction smoothly and continuously. The aerodynamic load is derived by using the first-order piston theory that including the curvature correction term. According to von Karman type nonlinear geometric relations, first-order shear deformation theory, Hamilton principle, the nonlinear equations of motion for the FGM truncated conical shell are established. Furthermore, the nonlinear

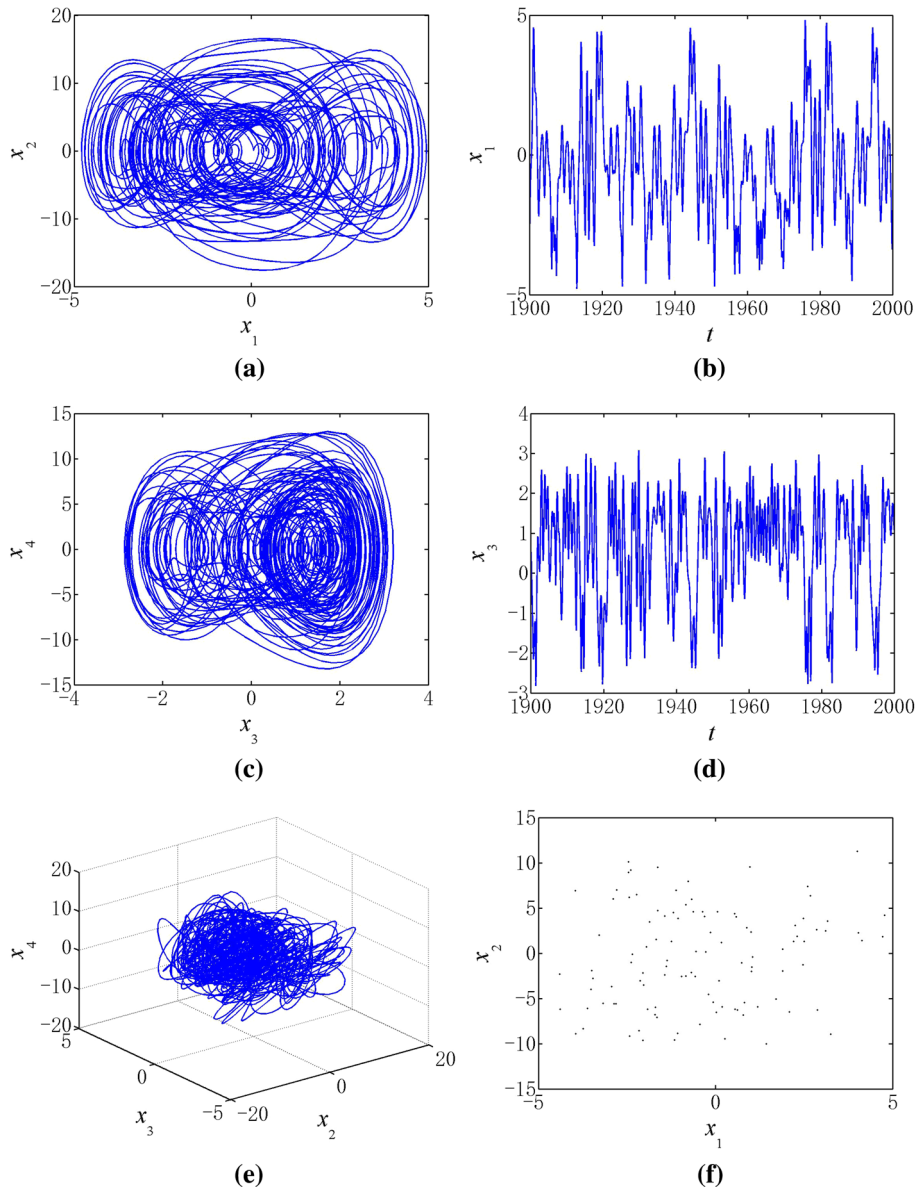

Fig. 16 The chaotic motion of the FGM truncated conical shell is given when $\eta = 5$, $M_a = 2$ and $p_1 = 100$

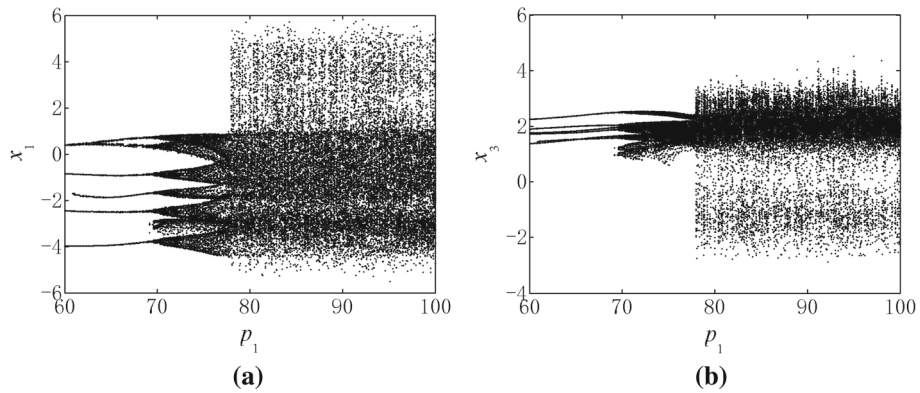

Fig. 17 The bifurcation diagram of the truncated FGM conical shell for in-plane load p_1 is obtained when exponent of volume fraction for the ceramic $\eta = 5$ and Mach number $M_a = 3$

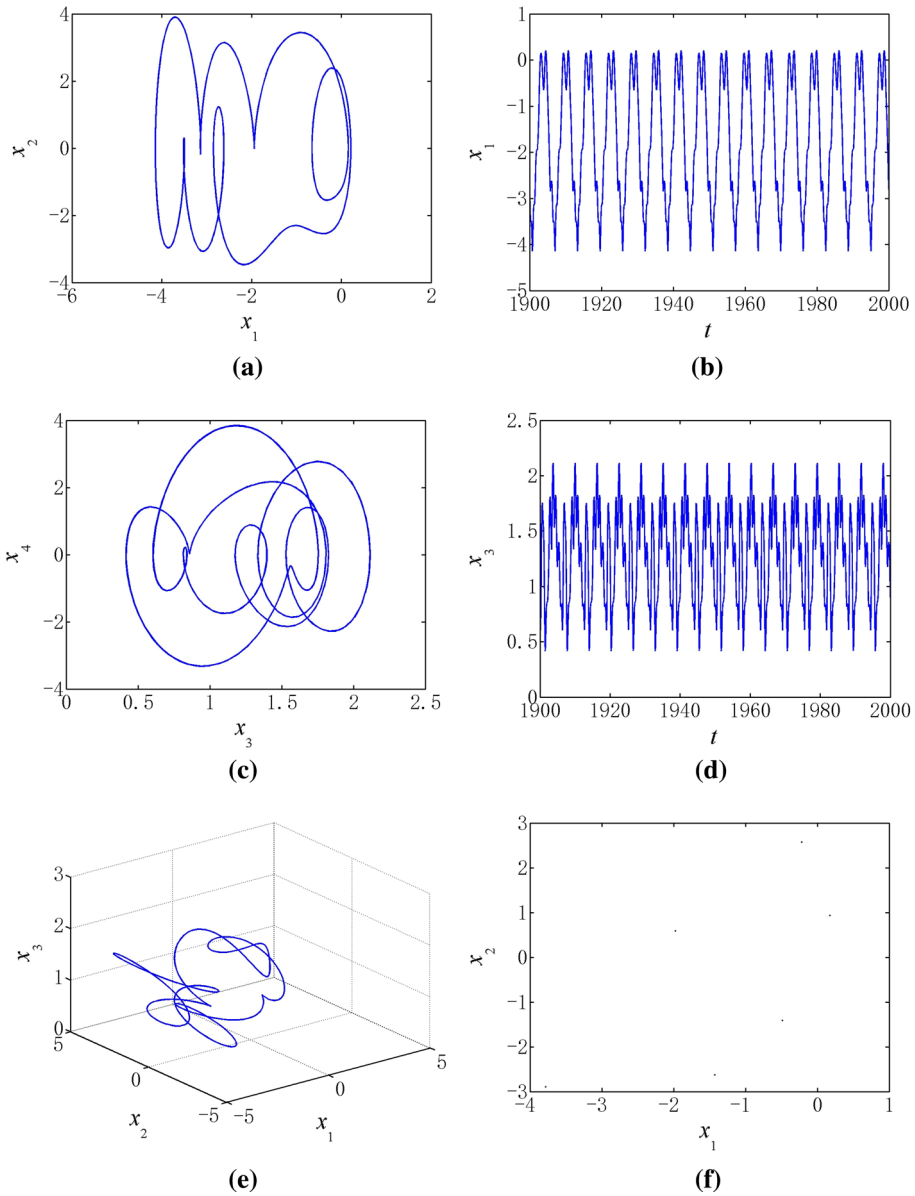

Fig. 18 The period motion of the FGM truncated conical shell is given when $\eta = 5$, $M_a = 3$ and $p_1 = 60$

equations of motion are reduced into a system of the ordinary differential equation by utilizing Galerkin procedure. The multiple scales method is used to obtain the averaged equations for the FGM truncated conical shell under the relations of 1:2 internal resonance and 1/2 subharmonic resonance.

The frequency–amplitude responses are investigated by solving the four-dimensional averaged equations. It is found that there are hardening-spring characteristics for the FGM truncated conical shell under the different cases. With the increase in Mach number or in-plane load, the nonlinear resonance characteristics become stronger. When the exponent of volume fraction or the damping coefficient decreases, the nonlinear resonance characteristics of the truncated FGM conical shell gets stronger and the amplitudes of two modes become larger.

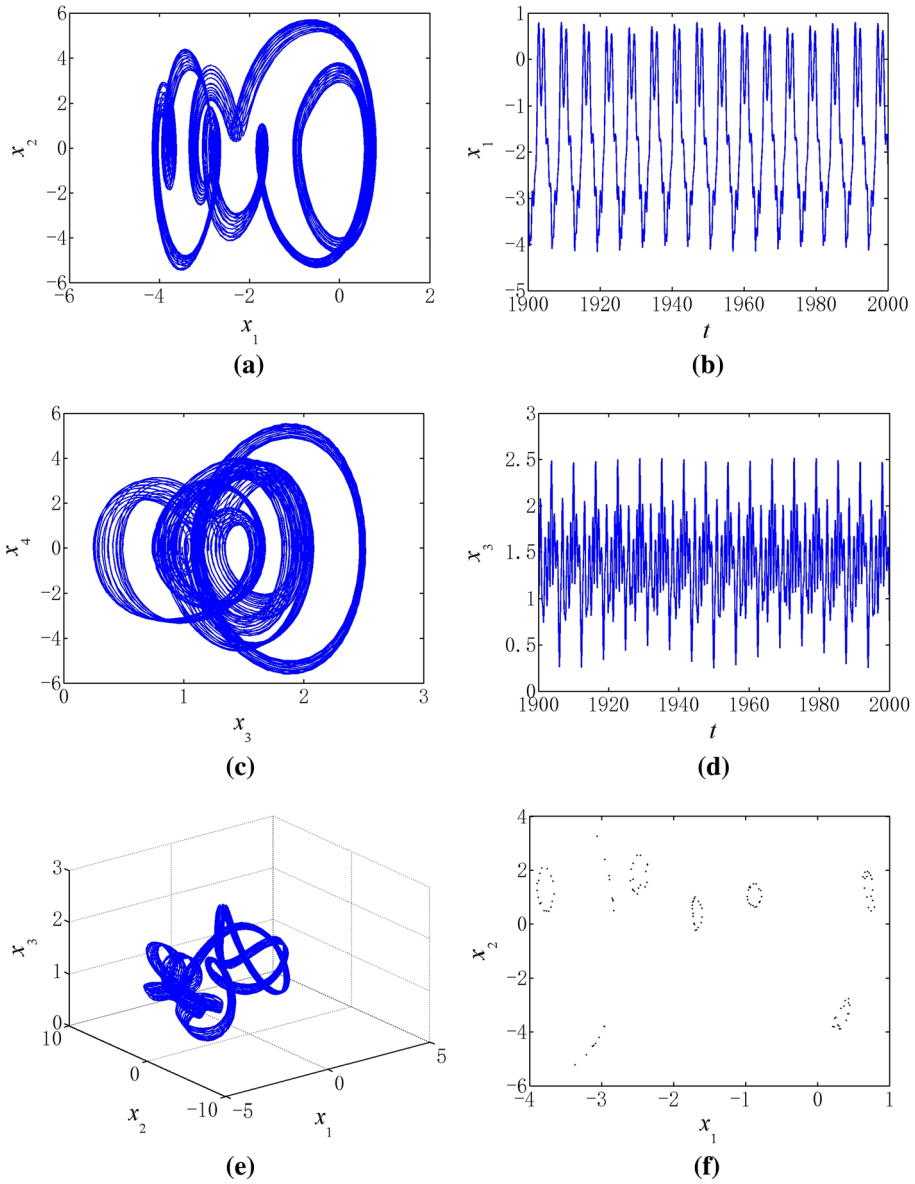

Fig. 19 The quasi-period motion of the FGM truncated conical shell is given when $\eta = 5$, $M_a = 3$ and $p_1 = 75$

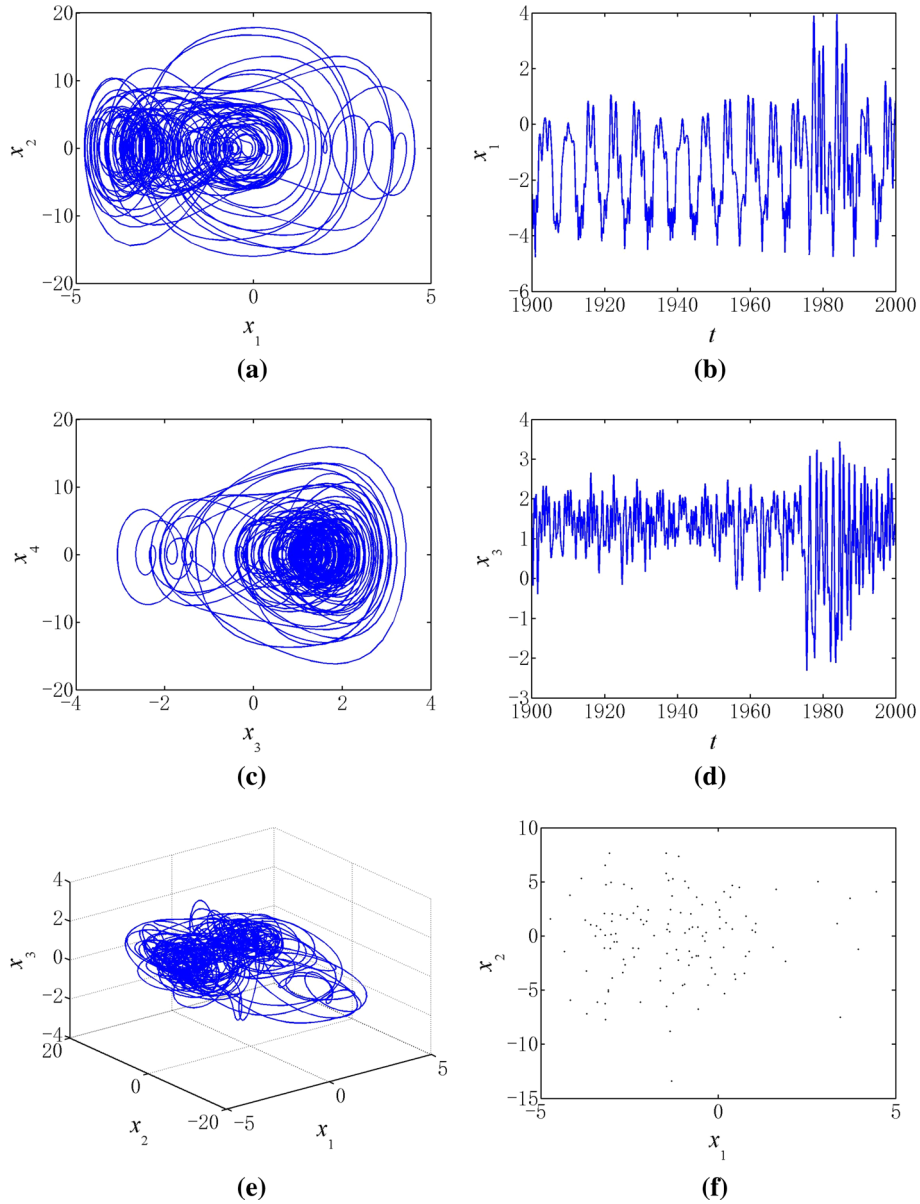

Fig. 20 The chaotic motion of the FGM truncated conical shell is given when $\eta = 5$, $M_a = 3$ and $p_1 = 100$

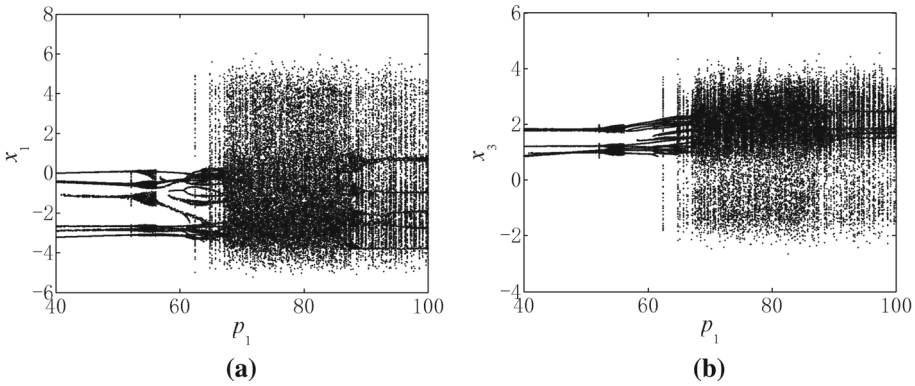

Fig. 21 The bifurcation diagram of the truncated FGM conical shell for in-plane load p_1 is obtained when exponent of volume fraction for the ceramic $\eta = 1$ and Mach number $M_a = 2$

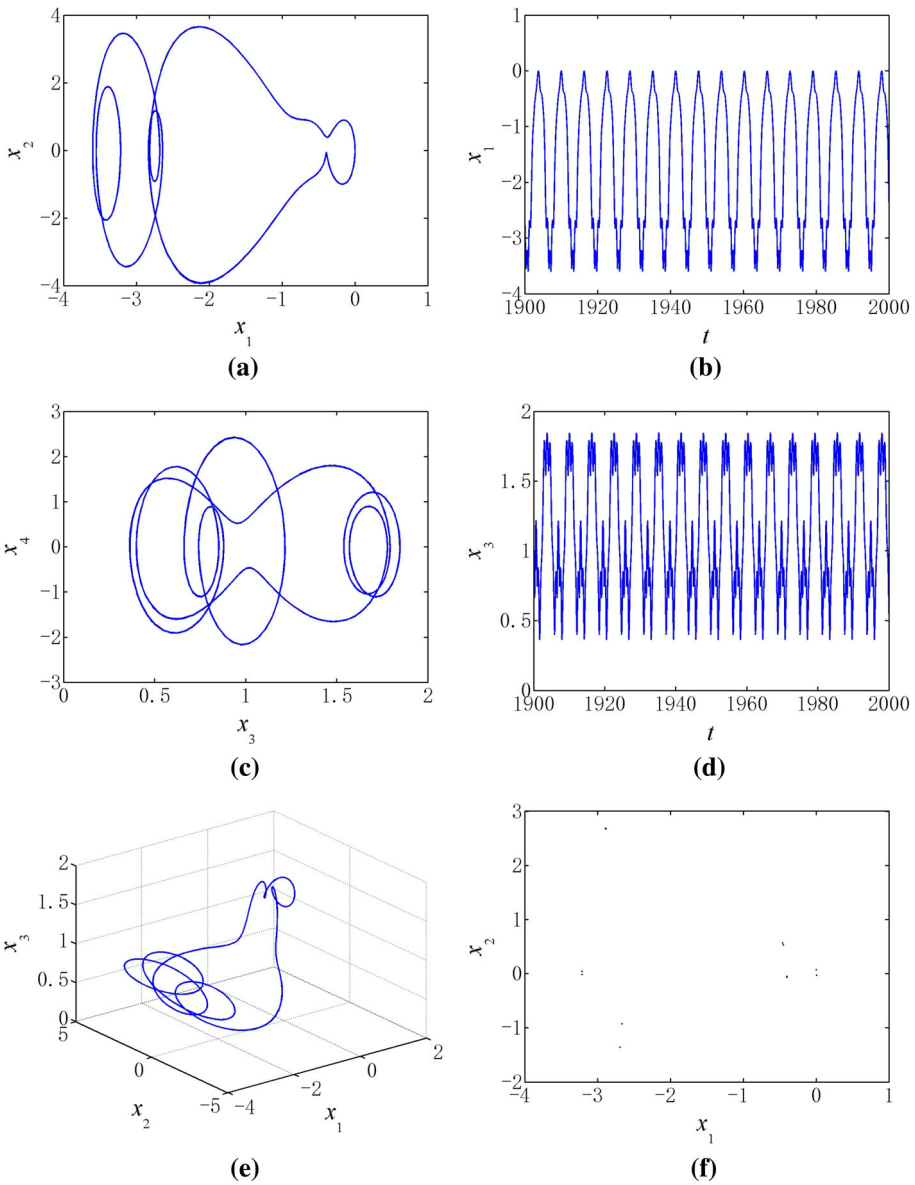

Fig. 22 The period motion of the FGM truncated conical shell is given when $\eta = 1$, $M_a = 2$ and $p_1 = 40$

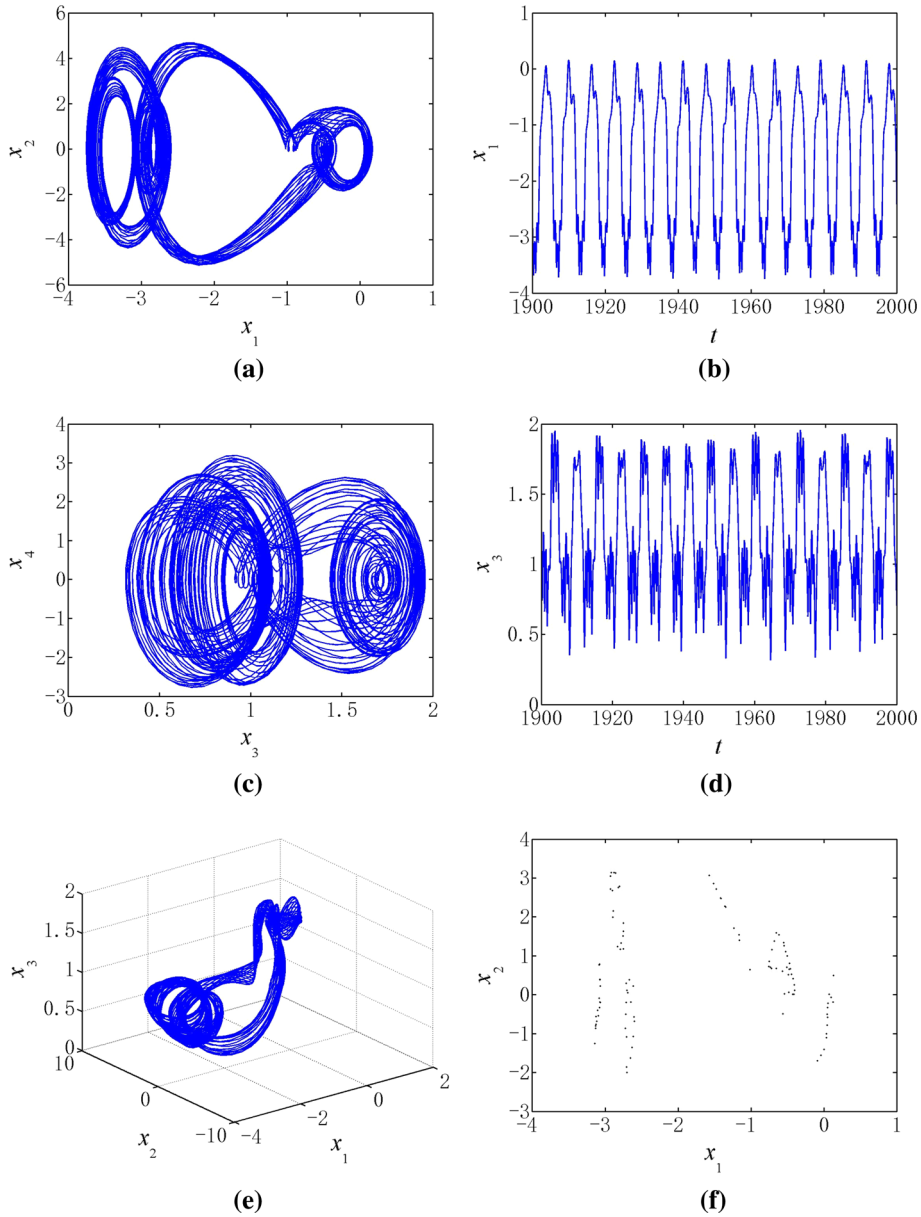

Fig. 23 The quasi-period motion of the FGM truncated conical shell is given when $\eta = 1$, $M_a = 2$ and $p_1 = 55$

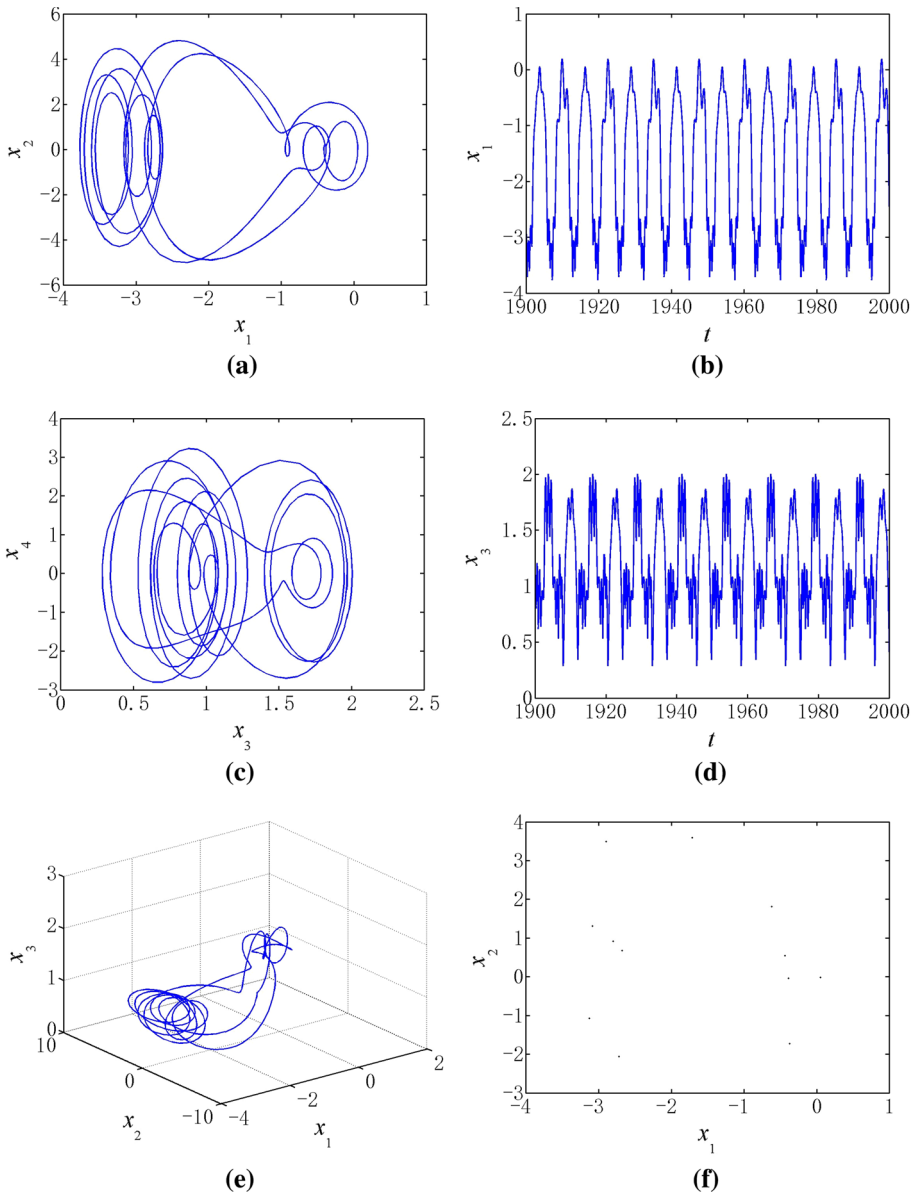

Fig. 24 The period motion of the FGM truncated conical shell is given when $\eta = 1$, $M_a = 2$ and $p_1 = 60$

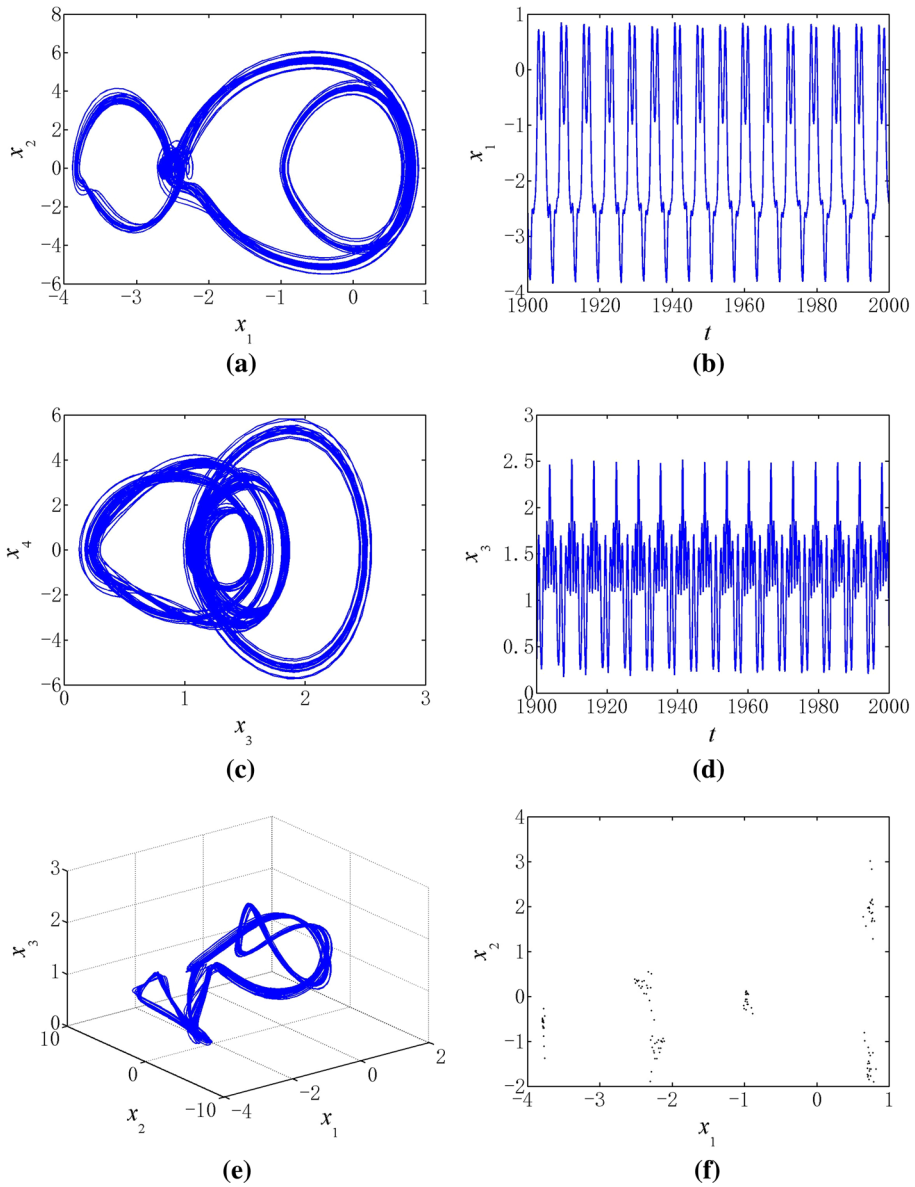

Fig. 25 The quasi-period motion of the FGM truncated conical shell is given when $\eta = 1$, $M_a = 2$ and $p_1 = 64$

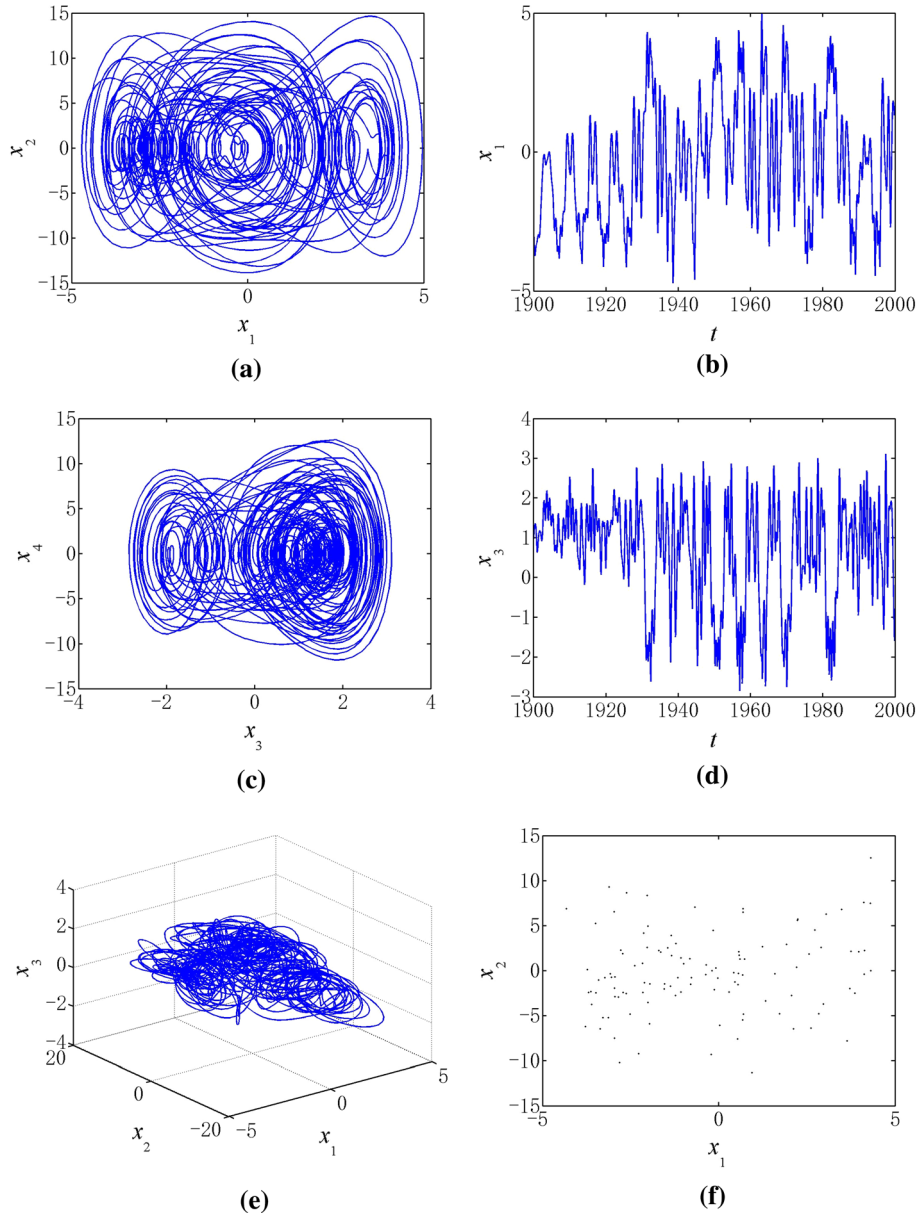

Fig. 26 The chaotic motion of the FGM truncated conical shell is given when $\eta = 1$, $M_a = 2$ and $p_1 = 100$

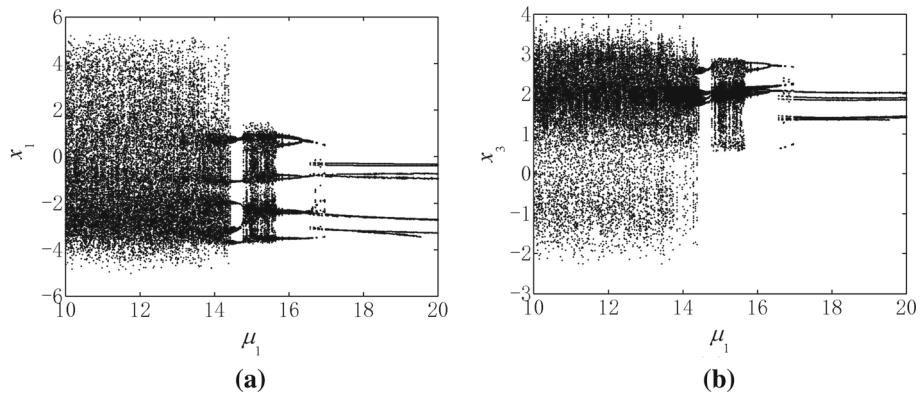

Fig. 27 The bifurcation diagram of the truncated FGM conical shell for damping coefficient μ_1 is obtained when exponent of volume fraction for the ceramic $\eta = 5$, in-plane load $p_1 = 100$ and Mach number $M_a = 3$

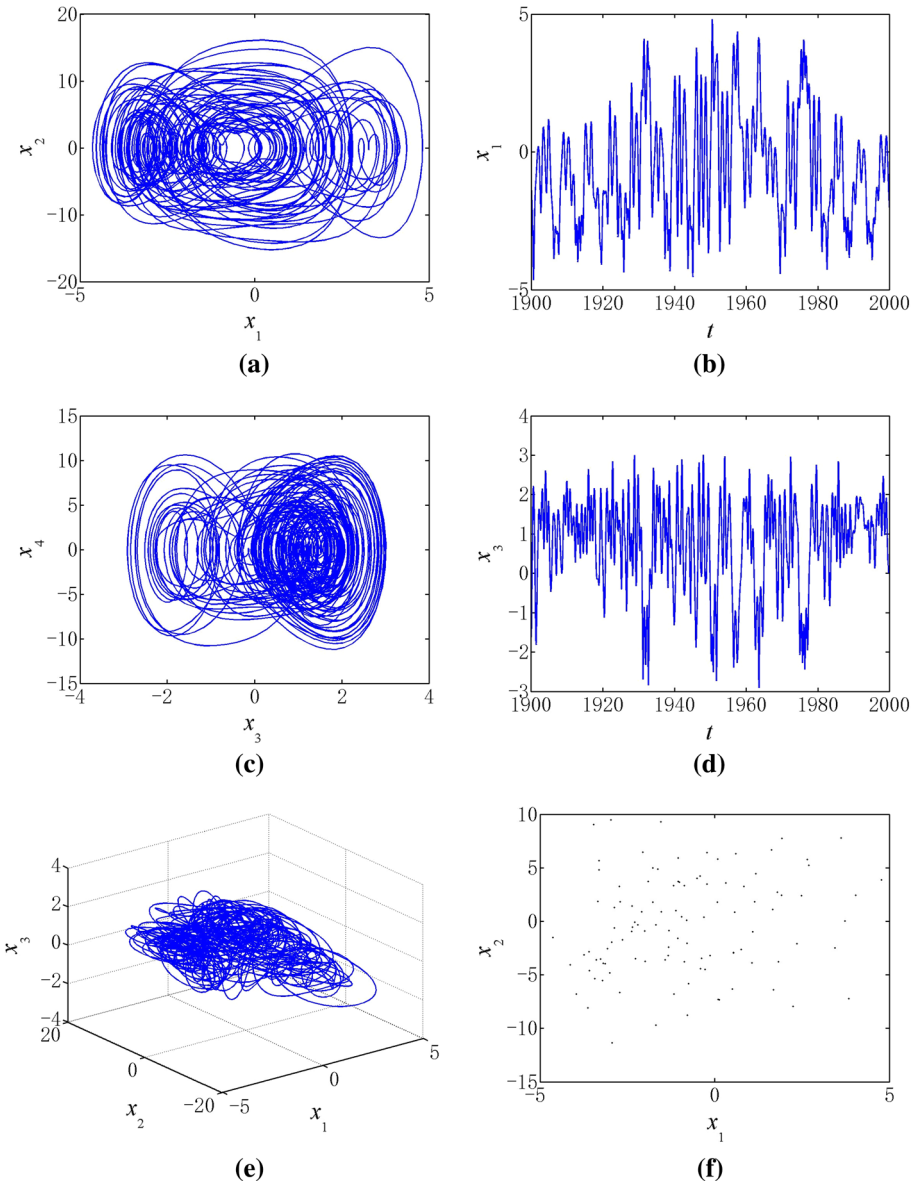

Fig. 28 The chaotic motion of the FGM truncated conical shell is given when $\mu_1 = 10$, $\eta = 5$, $M_a = 3$ and $p_1 = 100$

The complex nonlinear motion responses of the FGM truncated conical shell have been discussed in detail. It is observed that when in-plane load or damping coefficient increase, the periodic, the quasi-period and the chaotic motions occur for the FGM truncated conical shell. With the increase of the Mach number, the quasi-period motion and the chaotic motion both occur in advance. It is because of that with the increase of Mach number, aerodynamic heating creates higher temperature, and stiffness of the FGM truncated conical shell decreases. At the same time, the influence of the aerodynamic force on the nonlinear motion responses is greater. The chaotic motion yields earlier when the exponent of the volume fraction increases. It is due to that the increasing of the exponent of the volume fraction may cause smaller Young's modulus and greater thermal expansion coefficient of the FGM truncated conical shell.

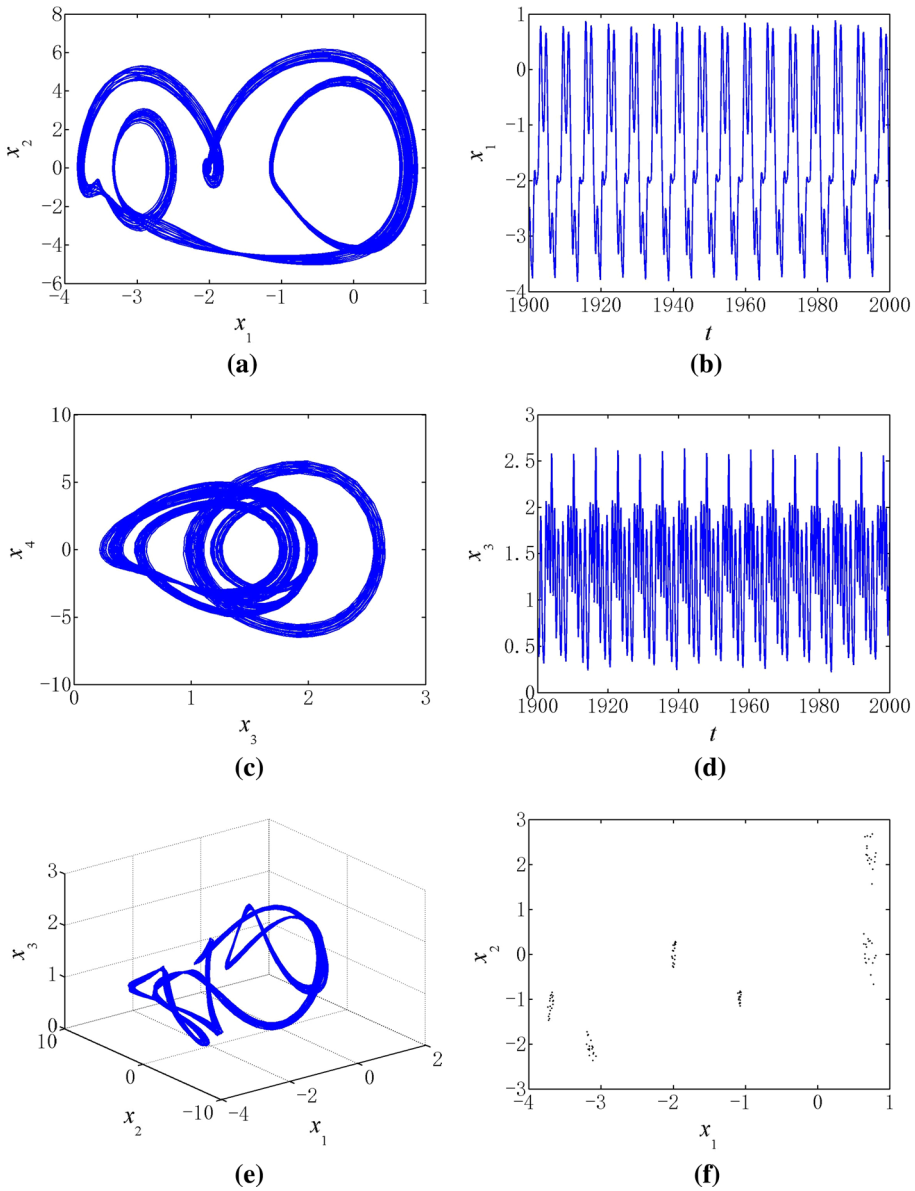

Fig. 29 The period motion of the FGM truncated conical shell is given when $\mu_1 = 14.6$, $\eta = 5$, $M_a = 3$ and $p_1 = 100$

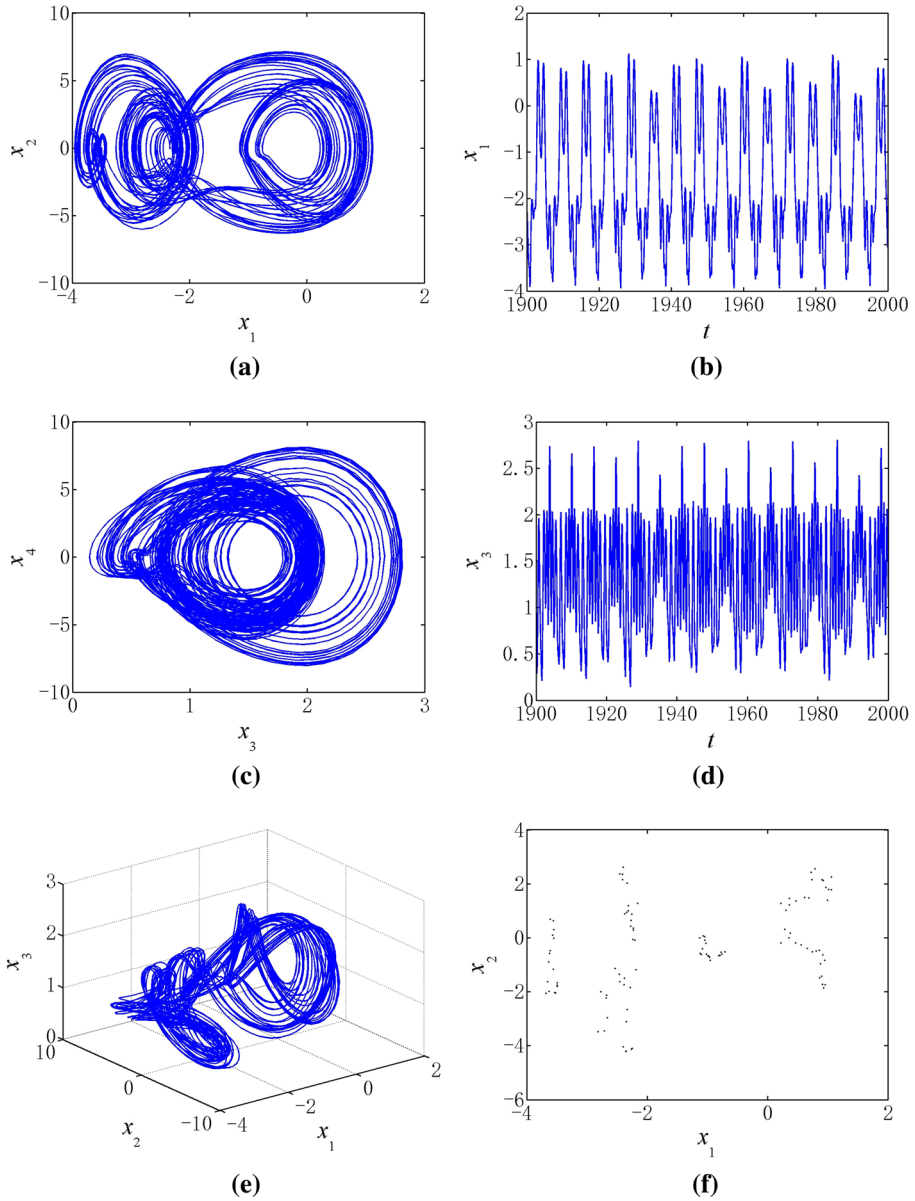

Fig. 30 The quasi-period motion of the FGM truncated conical shell is given when $\mu_1 = 15$, $\eta = 5$, $M_a = 3$ and $p_1 = 100$

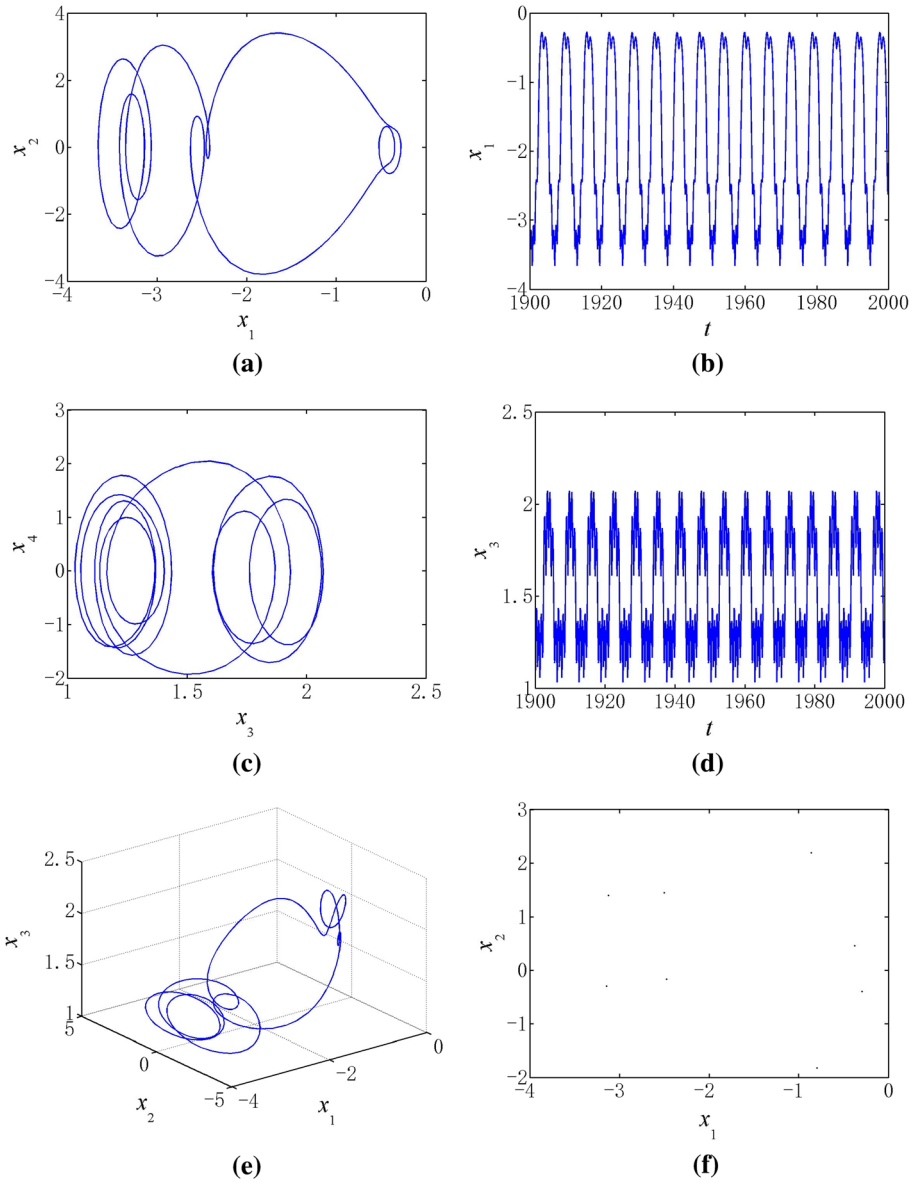

Fig. 31 The period motion of the FGM truncated conical shell is given when $\mu_1 = 20$, $\eta = 5$, $M_a = 3$ and $p_1 = 100$

Acknowledgements The authors acknowledge the financial support of National Natural Science Foundation of China through Grant Nos. 11872127 and 11832002, Qin Xin Talents Cultivation Program, Beijing Information Science & Technology University QXTCP A201901. Project of High-level Innovative Team Building Plan for Beijing Municipal Colleges and Universities No. IDHT20180513.

Compliance with ethical standards

Conflict of interest The authors declared that they have no conflicts of interest to this work.

Appendix A

Nonlinear equations in form of generalized displacements are listed, as follows

$$
\begin{aligned}
&A_{11}\frac{\partial^2 u_0}{\partial x^2}+\Re^2 A_{66}\frac{\partial^2 u_0}{\partial \theta^2}+\Re A_{11}\frac{\partial u_0}{\partial x}\sin\beta-\Re^2 A_{22}u_0\cos^2\beta+\Re\left(A_{12}+A_{66}\right)\frac{\partial^2 v_0}{\partial x\partial\theta}\\
&-\Re^2\left(A_{22}+A_{66}\right)\frac{\partial v_0}{\partial\theta}\sin\beta+\Re^2 A_{66}\frac{\partial^2 w_0}{\partial\theta^2}\frac{\partial w_0}{\partial x}+\Re^2\left(A_{12}+A_{66}\right)\frac{\partial^2 w_0}{\partial x\partial\theta}\frac{\partial w_0}{\partial\theta}\\
&+2\Re\left(A_{11}-A_{12}\right)\frac{\partial^2 w_0}{\partial x^2}\sin\beta-2\Re^3\left(A_{12}-A_{22}\right)\frac{\partial^2 w_0}{\partial\theta^2}\sin\beta+\Re A_{12}\frac{\partial w_0}{\partial x}\cos\beta\\
&-\Re^2 A_{22}w_0\sin\beta\cos\beta+B_{11}\frac{\partial^2\varphi_x}{\partial x^2}+\Re^2 B_{66}\frac{\partial^2\varphi_x}{\partial\theta^2}+\Re B_{11}\frac{\partial\varphi_x}{\partial x}\sin\beta-\Re^2 B_{22}\varphi_x\sin^2\beta\\
&-\Re^2\left(B_{22}+B_{66}\right)\frac{\partial\varphi_\theta}{\partial\theta}\sin\beta+\Re\left(B_{12}+B_{66}\right)\frac{\partial^2\varphi_\theta}{\partial x\partial\theta}+A_{11}\frac{\partial^2 w_0}{\partial x^2}\frac{\partial w_0}{\partial x}\\
&+\Re N_{xx}^T\sin\beta-\Re N_{\theta\theta}^T\sin\beta=I_0\ddot{u}_0+I_1\ddot{\varphi}_x,
\end{aligned}
\tag{A1}
$$

$$
\begin{aligned}
&\Re\left(A_{12}+A_{66}\right)\frac{\partial^2 u_0}{\partial x\partial\theta}+\Re^2\left(A_{22}+A_{66}\right)\frac{\partial u_0}{\partial\theta}\sin\beta+A_{66}\frac{\partial^2 v_0}{\partial x^2}+\Re^2 A_{22}\frac{\partial^2 v_0}{\partial\theta^2}\\
&-\Re^2\left(KA_{44}\cos^2\beta+A_{66}\sin^2\beta\right)v_0+\Re A_{66}\frac{\partial w_0}{\partial\theta}\frac{\partial^2 w_0}{\partial x^2}+\Re^3 A_{22}\frac{\partial^2 w_0}{\partial\theta^2}\frac{\partial w_0}{\partial\theta}\\
&+\Re\left(A_{12}+A_{66}\right)\frac{\partial^2 w_0}{\partial x\partial\theta}\frac{\partial w_0}{\partial x}+\Re^2 A_{66}\frac{\partial w_0}{\partial\theta}\frac{\partial w_0}{\partial x}\sin\beta+\Re^2 A_{22}\frac{\partial w_0}{\partial\theta}\cos\beta\\
&+\Re\left(B_{12}+B_{66}\right)\frac{\partial^2\varphi_x}{\partial x\partial\theta}+\Re^2\left(B_{22}+B_{66}\right)\frac{\partial\varphi_x}{\partial\theta}\sin\beta+\Re B_{66}\frac{\partial\varphi_\theta}{\partial x}\sin\beta+\Re B_{22}\frac{\partial^2\varphi_\theta}{\partial\theta^2}\\
&+\Re A_{66}\frac{\partial v_0}{\partial x}\sin\beta+\Re^2 KA_{44}\frac{\partial w_0}{\partial\theta}\cos\beta+\left(\Re KA_{44}\cos\beta-\Re^2 B_{66}\sin^2\beta\right)\varphi_\theta\\
&=I_0\ddot{v}_0+I_1\ddot{\varphi}_\theta,
\end{aligned}
\tag{A2}
$$

$$
\begin{aligned}
&2\Re^2 B_{66}\frac{\partial^2 w_0}{\partial x\partial\theta}\frac{\partial\varphi_x}{\partial\theta}+0.5\Re^2 A_{11}\left(\frac{\partial w_0}{\partial x}\right)^3\sin\beta-\Re N_{\theta\theta}^T\cos\beta+\Re\left(B_{11}+B_{22}\right)\frac{\partial\varphi_x}{\partial x}\frac{\partial w_0}{\partial x}\\
&-\Re^2 A_{66}\frac{\partial v_0}{\partial\theta}\frac{\partial w_0}{\partial x}\sin\beta-\Re^3\left(A_{12}+A_{66}\right)\frac{\partial^2 w_0}{\partial\theta^2}\frac{\partial w_0}{\partial x}+2\Re^2\left(A_{12}+2A_{66}\right)\frac{\partial^2 w_0}{\partial x\partial\theta}\frac{\partial w_0}{\partial\theta}\frac{\partial w_0}{\partial x}\\
&-\Re^2 B_{66}\frac{\partial\varphi_\theta}{\partial x}\frac{\partial w_0}{\partial x}\sin\beta+A_{11}\frac{\partial^2 u_0}{\partial x^2}\frac{\partial w_0}{\partial x}+B_{11}\frac{\partial^2\varphi_x}{\partial x^2}\frac{\partial w_0}{\partial x}+\Re\left(A_{12}+A_{66}\right)\frac{\partial^2 v_0}{\partial x\partial\theta}\frac{\partial w_0}{\partial x}\\
&+\Re\left(B_{12}+B_{66}\right)\frac{\partial^2\varphi_\theta}{\partial x\partial\theta}\frac{\partial w_0}{\partial x}+\Re^2 A_{66}\frac{\partial^2 u_0}{\partial\theta^2}\frac{\partial w_0}{\partial x}+\Re\left(KA_{55}+N_{xx}^T\right)\frac{\partial w_0}{\partial x}\sin\beta\\
&+\frac{3}{2}A_{11}\frac{\partial^2 w_0}{\partial x^2}\left(\frac{\partial w_0}{\partial x}\right)^2+0.5\Re^2\left(A_{12}+2A_{66}\right)\frac{\partial^2 w_0}{\partial\theta^2}\left(\frac{\partial w_0}{\partial x}\right)^2+0.5\Re^2 A_{12}\left(\frac{\partial w_0}{\partial x}\right)^2\cos\beta\\
&+\Re\left(A_{11}+A_{12}\right)\frac{\partial w_0}{\partial x}\frac{\partial u_0}{\partial x}\sin\beta+\Re^2 A_{12}\frac{\partial^2 w_0}{\partial\theta^2}\frac{\partial u_0}{\partial x}-A_{12}\frac{\partial u_0}{\partial x}\cos\beta+A_{11}\frac{\partial^2 w_0}{\partial x^2}\frac{\partial u_0}{\partial x}\\
&2\Re A_{66}\frac{\partial^2 w_0}{\partial x\partial\theta}\frac{\partial v_0}{\partial x}-\Re^2 A_{66}\frac{\partial w_0}{\partial\theta}\frac{\partial v_0}{\partial x}+\Re A_{12}\frac{\partial^2 w_0}{\partial x^2}w_0\cos\beta+\Re^3 A_{22}\frac{\partial^2 w_0}{\partial\theta^2}w_0\cos\beta
\end{aligned}
$$

$$
\begin{aligned}
&-\Re^2 A_{22} w_0 \cos\beta + \Re B_{12}\frac{\partial^2 w_0}{\partial x^2}\varphi_x \sin\beta + \Re^3 B_{22}\frac{\partial^2 w_0}{\partial \theta^2}\varphi_x \sin\beta \\
&+\left(\Re K A_{55} - \Re^2 B_{22}\cos\beta\right)\varphi_x \sin\beta + \Re^3 B_{66}\frac{\partial w_0}{\partial \theta}\varphi_\theta \sin^2\beta - \Re^2 B_{66}\frac{\partial^2 w_0}{\partial x \partial \theta}\varphi_\theta \sin\beta \\
&+\Re^3 A_{22}\frac{\partial^2 w_0}{\partial \theta^2}u_0 \sin\beta - \Re^3 A_{22} u_0 \sin\beta\cos\beta + \Re^2 A_{12}\frac{\partial^2 w_0}{\partial x^2}u_0 \sin\beta \\
&+\Re^3 A_{66}\frac{\partial w_0}{\partial \theta}v_0 \sin^2\beta - 2\Re^2 A_{66}\frac{\partial^2 w_0}{\partial x \partial \theta}v_0 \sin\beta + \Re^2\left(K A_{44} + N^T_{\theta\theta}\right)\frac{\partial^2 w_0}{\partial \theta^2} \\
&+\Re^3\left(B_{22} - B_{66}\right)\frac{\partial \varphi_x}{\partial \theta}\frac{\partial w_0}{\partial \theta} + \Re A_{66}\frac{\partial^2 v_0}{\partial x^2}\frac{\partial w_0}{\partial \theta} + \Re B_{66}\frac{\partial^2 \varphi_\theta}{\partial x^2}\frac{\partial w_0}{\partial \theta} \\
&+\Re^2\left(B_{12} + B_{66}\right)\frac{\partial^2 \varphi_x}{\partial x \partial \theta}\frac{\partial w_0}{\partial \theta} + \Re^3 A_{66}\frac{\partial^2 v_0}{\partial \theta^2}\frac{\partial w_0}{\partial \theta} + \Re^3 B_{22}\frac{\partial^2 \varphi_\theta}{\partial \theta^2}\frac{\partial w_0}{\partial \theta} \\
&+\left(K A_{55} + N^T_{xx} - p\cos\Omega t\right)\frac{\partial^2 w_0}{\partial x^2} + 0.5\Re\left(A_{12} + 2A_{66}\right)\frac{\partial^2 w_0}{\partial x^2}\left(\frac{\partial w_0}{\partial \theta}\right)^2 \\
&+0.5\Re^3 A_{22}\frac{\partial^2 w_0}{\partial \theta^2}\left(\frac{\partial w_0}{\partial \theta}\right)^2 + \Re A_{12}\frac{\partial^2 w_0}{\partial x^2}\frac{\partial v_0}{\partial \theta} + \Re^3 A_{22}\frac{\partial^2 w_0}{\partial \theta^2}\frac{\partial v_0}{\partial \theta} + K A_{55}\frac{\partial \varphi_x}{\partial x} \\
&-\Re^2\left(K A_{44} + A_{22}\right)\frac{\partial v_0}{\partial \theta}\cos\beta + B_{11}\frac{\partial^2 w_0}{\partial x^2}\frac{\partial \varphi_x}{\partial x} - \Re B_{12}\frac{\partial \varphi_x}{\partial x}\cos\beta + \Re^2 B_{12}\frac{\partial^2 w_0}{\partial \theta^2}\frac{\partial \varphi_x}{\partial x} \\
&+2\Re B_{66}\frac{\partial^2 w_0}{\partial x \partial \theta}\frac{\partial \varphi_\theta}{\partial x} - \Re^2 B_{66}\frac{\partial w_0}{\partial \theta}\frac{\partial \varphi_\theta}{\partial x}\sin\beta + \Re^3\left(A_{22} - A_{66}\right)\frac{\partial w_0}{\partial \theta}\frac{\partial u_0}{\partial \theta}\sin\beta \\
&+\Re^2 B_{66}\frac{\partial^2 \varphi_x}{\partial \theta^2}\frac{\partial w_0}{\partial x} + \Re^2\left(A_{12} + A_{66}\right)\frac{\partial^2 u_0}{\partial x \partial \theta}\frac{\partial w_0}{\partial \theta} + 0.5\Re^3 A_{22}\frac{\partial^2 w_0}{\partial \theta^2}\cos\beta \\
&+2\Re^3 A_{66}\frac{\partial^2 w_0}{\partial x \partial \theta}\frac{\partial u_0}{\partial \theta} + P_a - \kappa\dot{w}_0 = I_0\ddot{w}_0,
\end{aligned}
\tag{A3}
$$

$$
\begin{aligned}
&B_{11}\frac{\partial^2 u_0}{\partial x^2} + \Re^2 B_{66}\frac{\partial^2 u_0}{\partial \theta^2} + \Re B_{11}\frac{\partial u_0}{\partial x}\sin\beta - \Re^2 B_{22} u_0 \sin^2\beta + \Re\left(B_{12} + B_{66}\right)\frac{\partial^2 v_0}{\partial x \partial \theta} \\
&-\Re^2\left(B_{22} + B_{66}\right)\frac{\partial v_0}{\partial \theta}\sin\beta + 0.5\Re^2\left(B_{11} - B_{12}\right)\frac{\partial^2 w_0}{\partial x^2}\sin\beta - \Re^2 B_{22} w_0 \sin\beta\cos\beta \\
&+\Re B_{12}\frac{\partial w_0}{\partial x}\cos\beta + B_{11}\frac{\partial^2 w_0}{\partial x^2}\frac{\partial w_0}{\partial x} + \Re^2 B_{66}\frac{\partial^2 w_0}{\partial \theta^2}\frac{\partial w_0}{\partial x} - K A_{55}\frac{\partial w_0}{\partial x} \\
&-0.5\Re^2\left(B_{12} + B_{22}\right)\frac{\partial^2 w_0}{\partial \theta^2}\sin\beta + \Re^2\left(B_{12} + B_{66}\right)\frac{\partial^2 w_0}{\partial x \partial \theta}\frac{\partial w_0}{\partial \theta} - \left(K A_{55} + \frac{1}{R^2}D_{22}\right)\varphi_x \\
&+\Re D_{11}\frac{\partial \varphi_x}{\partial x}\sin\beta + \Re^2 D_{66}\frac{\partial^2 \varphi_x}{\partial \theta^2} + D_{11}\frac{\partial^2 \phi_x}{\partial x^2} + \Re\left(D_{12} + D_{66}\right)\frac{\partial^2 \varphi_x}{\partial x \partial \theta} \\
&-\Re^2\left(D_{22} + D_{66}\right)\frac{\partial \varphi_\theta}{\partial \theta}\sin\beta + \Re M^T_{xx}\sin\beta - \Re M^T_{\theta\theta}\sin\beta = I_1\ddot{u}_0 + I_2\ddot{\varphi}_x,
\end{aligned}
\tag{A4}
$$

$$
\begin{aligned}
&\Re\left(B_{12} + B_{66}\right)\frac{\partial^2 u_0}{\partial x \partial \theta} + \Re^2\left(B_{22} + B_{66}\right)\frac{\partial u_0}{\partial \theta}\sin\beta + B_{66}\frac{\partial^2 v_0}{\partial x^2} + \Re^2 B_{22}\frac{\partial^2 v_0}{\partial \theta^2} \\
&\quad+\left(\Re K A_{44}\cos\beta - \Re^2 B_{66}\sin^2\beta\right)v_0 + \Re^2 B_{66}\frac{\partial w_0}{\partial x}\frac{\partial w_0}{\partial \theta}\sin\beta \\
&\quad+\left(\Re^2 B_{22}\cos\beta - \Re K A_{44}\right)\frac{\partial w_0}{\partial \theta} + \Re^3 B_{22}\frac{\partial^2 w_0}{\partial \theta^2}\frac{\partial w_0}{\partial \theta} + \Re B_{66}\frac{\partial^2 w_0}{\partial x^2}\frac{\partial w_0}{\partial \theta} \\
&\quad+\Re^2\left(D_{22} + D_{66}\right)\frac{\partial \varphi_\theta}{\partial \theta} + \Re^2 D_{22}\frac{\partial^2 \varphi_\theta}{\partial \theta^2} + \Re D_{66}\frac{\partial \varphi_\theta}{\partial x} - \left(K A_{44} + \Re^2 D_{66}\sin^2\beta\right)\varphi_\theta \\
&\quad+\Re B_{66}\frac{\partial v_0}{\partial x}\sin\beta + \Re\left(B_{12} + B_{66}\right)\frac{\partial^2 w_0}{\partial x \partial \theta}\frac{\partial w_0}{\partial x} + \Re\left(D_{12} + D_{66}\right)\frac{\partial^2 \varphi_x}{\partial x \partial \theta} + D_{66}\frac{\partial^2 \varphi_\theta}{\partial x^2} \\
&= I_1\ddot{v}_0 + I_2\ddot{\varphi}_\theta.
\end{aligned}
\tag{A5}
$$

References

1. Sofiyev, A.H.: The vibration and stability behavior of freely supported FGM conical shells subjected to external pressure. Compos. Struct. **89**, 56–366 (2009)
2. Sofiyev, A.H., Kuruoglu, N.: On a problem of the vibration of functionally graded conical shells with mixed boundary conditions. Compos. B Eng. **70**, 122–130 (2015)
3. Yang, S.W., Hao, Y.X., Zhang, W., Li, S.B.: Nonlinear dynamic behavior of functionally graded truncated conical shell under complex loads. Int. J. Bifurc. Chaos **25**, 1550025 (2015)
4. Yang, S.W., Zhang, W., Hao, Y.X., Niu, Y.: Nonlinear vibrations of FGM truncated conical shell under aerodynamics and in-plane force along meridian near internal resonances. Thin Walled Struct. **142**, 369–391 (2019)
5. Akbari, M., Kiani, Y., Eslami, M.R.: Thermal buckling of temperature-dependent FGM conical shells with arbitrary edge supports. Acta Mech. **226**, 897–915 (2015)
6. Ansari, R., Hasrati, E., Torabi, J.: Nonlinear vibration response of higher-order shear deformable FG-CNTRC conical shells. Compos. Struct. **222**, 110906 (2019)
7. Chan, D.Q., Anh, V.T.T., Duc, N.D.: Vibration and nonlinear dynamic response of eccentrically stiffened functionally graded composite truncated conical shells surrounded by an elastic medium in thermal environments. Acta Mech. **230**, 157–178 (2019)
8. Chan, D.Q., Quan, T.Q., Kim, S.E.: Nonlinear dynamic response and vibration of shear deformable piezoelectric functionally graded truncated conical panel in thermal environments. Eur. J. Mech. A Solids **77**, 103795 (2019)
9. Dai, Q.Y., Cao, Q.J., Chen, Y.S.: Frequency analysis of rotating truncated conical shells using the Haar wavelet method. Appl. Math. Model. **57**, 603–613 (2018)
10. Rahmani, M., Mohammadi, Y., Kakavand, F.: Vibration analysis of sandwich truncated conical shells with porous FG face sheets in various thermal surroundings. Steel Compos. Struct. **32**, 239–252 (2019)
11. Song, Z.Y., Cao, Q.J., Dai, Q.Y.: Free vibration of truncated conical shells with elastic boundary constraints and added mass. Int. J. Mech. Sci. **155**, 286–294 (2019)
12. Hao, Y.X., Niu, N., Zhang, W., Li, S.B., Yao, M.H., Wang, A.W.: Supersonic flutter analysis of FGM shallow conical panel accounting for thermal effects. Meccanica **53**, 95–109 (2018)
13. Hao, Y.X., Niu, N., Zhang, W., Yao, M.H., Li, S.B.: Nonlinear vibrations of FGM circular conical panel under in-plane and transverse excitation. J. Vib. Eng. Technol. **6**, 453–469 (2018)
14. Sofiyev, A.H.: Review of research on the vibration and buckling of the FGM conical shells. Compos. Struct. **211**, 301–317 (2019)
15. Jooybar, N., Malekzadeh, P., Fiouz, A., Vaghefi, M.: Thermal effect on free vibration of functionally graded truncated conical shell panels. Thin Walled Struct. **103**, 45–61 (2016)
16. Hao, Y.X., Yang, S.W., Zhang, W., Yao, M.H., Wang, A.W.: Flutter of high-dimension nonlinear system for a FGM truncated conical shell. Mech. Adv. Mater. Struct. **25**, 47–61 (2018)
17. Izadi, M.H., Hosseini-Hashemi, S., Korayem, M.H.: Analytical and FEM solutions for free vibration of joined cross-ply laminated thick conical shells using shear deformation theory. Arch. Appl. Mech. **88**, 2231–2246 (2018)
18. Zhao, Y.K., Shi, D.Y., Meng, H.: A unified spectro-geometric-Ritz solution for free vibration analysis of conical-cylindrical-spherical shell combination with arbitrary boundary conditions. Arch. Appl. Mech. **87**, 961–988 (2017)
19. Deniz, A., Sofiyev, A.H.: The nonlinear dynamic buckling response of functionally graded truncated conical shells. J. Sound Vib. **332**, 978–992 (2013)
20. Sofiyev, A.H., Zerin, Z., Allahverdiev, B.P., Hui, D., Turan, F., Erdem, H.: The dynamic instability of FG orthotropic conical shells within the SDT. Steel Compos. Struct. **25**, 581–591 (2017)
21. Hoa, L.K., Hoai, B.T.T., Chan, D.Q.: Nonlinear thermomechanical postbuckling analysis of ES-FGM truncated conical shells resting on elastic foundations. Mech. Adv. Mater. Struct. **26**, 1089–1103 (2019)
22. Chan, D.Q., Nguyen, P.D., Quang, V.D.: Nonlinear buckling and post-buckling of functionally graded CNTs reinforced composite truncated conical shells subjected to axial load. Steel Compos. Struct. **31**, 243–259 (2019)
23. Chan, D.Q., Long, V.D., Duc, N.D.: Nonlinear buckling and postbuckling of FGM shear-deformable truncated conical shells reinforced by FGM stiffeners. Mech. Compos. Mater. **54**, 745–764 (2019)
24. Kiani, Y.: Buckling of functionally graded graphene reinforced conical shells under external pressure in thermal environment. Compos. B Eng. **156**, 128–137 (2019)
25. Jiao, P., Chen, Z.P., Li, Y.: Dynamic buckling analyses of functionally graded carbon nanotubes reinforced composite (FG-CNTRC) cylindrical shell under axial power-law time-varying displacement load. Compos. Struct. **220**, 784–797 (2019)
26. Talebitooti, M.: Analytical and finite-element solutions for the buckling of composite sandwich conical shell with clamped ends under external pressure. Arch. Appl. Mech. **87**, 59–73 (2017)
27. Dung, D.V., Chan, D.Q.: Analytical investigation on mechanical buckling of FGM truncated conical shells reinforced by orthogonal stiffeners based on FSDT. Compos. Struct. **159**, 827–841 (2017)
28. Zhao, X., Liew, K.M.: An element-free analysis of mechanical and thermal buckling of functionally graded conical shell panels. Comput. Methods Appl. Mech. Eng. **86**, 269–285 (2011)
29. Pasqua, M.F.D., Khakimova, R., Castro, S.G.P., Arbelo, M.A., Riccio, A.: Investigation on the geometric imperfections driven local buckling onset in composite conical shells. Appl. Compos. Mater. **23**, 879–897 (2016)
30. Talebitooti, M.: Analytical and finite-element solutions for the buckling of composite sandwich conical shell with clamped ends under external pressure. Arch. Appl. Mech. **87**, 1–15 (2016)
31. Maali, M., Showkati, H., Fatemi, S.M.: Investigation of the buckling behavior of conical shells under weld-induced imperfections. Thin Walled Struct. **57**, 13–24 (2012)
32. Sofiyev, A.H., Zerin, Z., Kuruoglu, N.: Thermoplastic buckling of FGM conical shells under non-linear temperature rise in the framework of the shear deformation theory. Compos. B Eng. **108**, 279–290 (2017)
33. Bich, D.H., Phuong, N.T., Tung, H.V.: Buckling of functionally graded conical panels under mechanical loads. Compos. Struct. **94**, 1379–1384 (2012)

34. Zhang, Y., Shi, D.: An exact Fourier series method for vibration analysis of elastically connected laminated composite double-beam system with elastic constraints. Mech. Adv. Mater. Struct. (2020). https://doi.org/10.1080/15376494.2020.1741750
35. Shi, D.Y., He, D., Wang, Q., Ma, C., Shu, H.: Free vibration analysis of closed moderately thick cross-ply composite laminated cylindrical shell with arbitrary boundary conditions. Materials **13**, 884 (2020)
36. He, D., Shi, D.Y., Wang, Q., Shuai, C.: Wave based method (WBM) for free vibration analysis of cross-ply composite laminated cylindrical shells with arbitrary boundaries. Compos. Struct. **213**, 284–298 (2019)
37. Zhang, H., Shi, D., Zha, S., Wang, Q.: A modified Fourier solution for sound-vibration analysis for composite laminated thin sector plate-cavity coupled system. Compos. Struct. **207**, 560–575 (2019)
38. Wang, Q., Shi, D., Liang, Q., Pang, F.: Free vibrations of composite laminated doubly-curved shells and panels of revolution with general elastic restraints. Appl. Math. Model. **46**, 227–262 (2017)
39. Jin, G., Ma, X., Shi, S., Ye, T., Liu, Z.: A modified Fourier series solution for vibration analysis of truncated conical shells with general boundary conditions. Appl. Acoust. **85**, 82–96 (2014)
40. Dai, L., Yang, T., Li, W.L., Du, J., Jin, G.: Dynamic analysis of circular cylindrical shells with general boundary condition using modified Fourier series method. J. Vib. Acoust. **134**, 041004 (2012)
41. Zhang, W., Liu, T., Xi, A., Wang, Y.N.: Resonant responses and chaotic dynamics of composite laminated circular cylindrical shell with membranes. J. Sound Vib. **423**, 65–99 (2018)
42. Sun, Y., Zhang, W., Yao, M.H.: Multi-pulse chaotic dynamics of circular mesh antenna with 1:2 internal resonance. Int. J. Appl. Mech. **9**, 1750060 (2017)
43. Zhang, W., Chen, J.E., Cao, D.X., Chen, L.H.: Nonlinear dynamic responses of a truss core sandwich plate. Compos. Struct. **108**, 367–386 (2014)
44. Hao, Y.X., Zhang, W., Yang, J.: Nonlinear dynamics of cantilever FGM cylindrical shell under 1:2 internal resonance relations. Mech. Adv. Mater. Struct. **20**, 819–833 (2013)
45. Amabili, M.: Nonlinear Vibrations and Stability of Shells and Plates. CU Press, New York (2008)
46. Mahmoudkhani, S., Haddadpour, H., Navazi, H.M.: Supersonic flutter prediction of functionally graded conical shells. Compos. Struct. **92**, 377–386 (2010)
47. Sabri, F., Lakis, A.A.: Hybrid finite element method applied to supersonic flutter of an empty or partially liquid-filled truncated conical shell. J. Sound Vib. **239**, 302–316 (2010)
48. Mehri, M., Asadi, H., Wang, Q.: On dynamic instability of a pressurized functionally graded carbon nanotube reinforced truncated conical shell subjected to yawed supersonic airflow. Compos. Struct. **153**, 938–951 (2016)
49. Praveen, G.N., Reddy, J.N.: Nonlinear transient thermoelastic analysis of functionally graded ceramic-metal plates. Int. J. Solids Struct. **35**, 4457–4476 (1998)
50. Pradhan, S.C., Loya, C.T., Lama, K.Y., Reddy, J.N.: Vibration characteristics of functionally graded cylindrical shells under various boundary conditions. Appl. Acoust. **61**, 111–129 (2000)
51. Reddy, J.N.: Mechanics of Laminated Composite Plates and Shells: Theory and Analysis. CRC Press, New York (2004)
52. Maleki, S., Tahani, M.: Non-linear analysis of fiber-reinforced open conical shell panels considering variation of thickness and fiber orientation under thermo-mechanical loadings. Compos. B Eng. **52**, 245–261 (2013)
53. Patel, B.P., Singh, S., Nath, Y.: Postbuckling characteristics of angle-ply laminated truncated circular conical shells. Commun. Nonlinear Sci. Numer. Simul. **13**, 1411–1430 (2008)
54. Navazi, H.M., Haddadpour, H.: Nonlinear aero-thermoelastic analysis of homogeneous and functionally graded plates in supersonic airflow using coupled models. Compos. Struct. **93**, 2554–2565 (2011)
55. Shen, H.S.: Postbuckling of shear deformable FGM cylindrical shells surrounded by an elastic medium. Int. J. Mech. Sci. **51**, 372–383 (2009)
56. Efraim, E., Eisenberger, M.: Exact vibration analysis of variable thickness thick annular isotropic and FGM plates. J. Sound Vib. **299**, 720–738 (2007)
57. Noseir, A., Reddy, J.N.: A study of non-linear dynamic equations of higher-order deformation plate theories. Int. J. Non Linear Mech. **26**, 233–249 (1991)
58. Bhimaraddi, A.: Large amplitude vibrations of imperfect antisymmetric angle-ply laminated plates. J. Sound Vib. **162**, 457–470 (1993)
59. Nayfeh, A.H., Mook, D.T.: Nonlinear Oscillations. Wiley, New York (1979)
60. Liew, K.M., Ng, T.Y., Zhao, X.: Free vibration analysis of conical shells via the element-free kp-Ritz method. J. Sound Vib. **281**, 627–645 (2005)
61. Kerboua, Y., Lakis, A.A., Hmila, M.: Vibration analysis of truncated conical shells subjected to flowing fluid. Appl. Math. Model. **34**, 791–809 (2010)
62. Najafov, A.M., Sofiyev, A.H.: The non-linear dynamics of FGM truncated conical shells surrounded by an elastic medium. Int. J. Mech. Sci. **66**, 33–44 (2013)
63. Shen, H.S.: Nonlinear vibration of shear deformable FGM cylindrical shells surrounded by an elastic medium. Compos. Struct. **94**, 1144–1154 (2012)